PEDIATRIC ALLERGY, IMMUNOLOGY, AND PULMONOLOGY
Volume 23, Number 1, 2010

DOI: 10.1089/ped.2010.0010

Imaging of Childhood Interstitial Lung Disease

R. Paul Guillerman, M.D.

The aphorism that children are not little adults certainly applies for the imaging of interstitial lung disease. Acquiring motion-free images of fine pulmonary structures at desired lung volumes is much more difficult in children than in adults. Several forms of interstitial lung disease are unique to children, and some forms of interstitial lung disease encountered in adults rarely, if ever, occur in children. Meticulous attention to imaging technique and specialized knowledge are required to properly perform and interpret chest imaging studies obtained for the evaluation of childhood interstitial lung disease (chILD). This review will address technique recommendations for imaging chILD, the salient imaging findings in various forms of chILD, and the efficacy of imaging in the diagnosis and management of chILD.

Introduction

Childhood interstitial lung disease (chILD) encompasses a heterogeneous group of rare diffuse lung diseases that can result in considerable morbidity and mortality. Although interstitial lung disease is an entrenched term in the vernacular, the associated disease processes may affect not only the interstitium but also the alveoli, airways, blood vessels, lymphatic channels, and pleural spaces. Classification of these diseases is based primarily on clinicopathologic patterns and expert opinion.

The American Thoracic Society/European Respiratory Society International Multidisciplinary Consensus Classification of the Idiopathic Interstitial Pneumonias developed for the adult population is inappropriate for chILD since it includes diseases that rarely, if ever, occur in children and omits several diseases that are unique to the pediatric population.[1] These diseases are incorporated in the classification scheme for diffuse lung disease in young children proposed by the chILD Research Cooperative and organized on the basis of the presumed etiology.[2] According to this novel scheme, unique diseases more prevalent in infancy include the diffuse developmental disorders (alveolar capillary dysplasia with misalignment of the pulmonary veins, congenital alveolar dysplasia), growth abnormalities (chronic neonatal lung disease, chromosomal disorders such as Down syndrome), pulmonary interstitial glycogenosis (PIG), neuroendocrine cell hyperplasia of infancy (NEHI), and genetic surfactant dysfunction disorders. Other categories in this scheme include disorders of the normal host (bronchiolitis obliterans, aspiration, eosinophilic pneumonia, hypersensitivity pneumonitis), disorders of the immunocompromised host (diffuse alveolar damage (DAD), opportunistic infection), disorders related to systemic disease (collagen-vascular diseases, capillaritis, storage diseases), and masquerading disorders such as pulmonary arterial hypertensive vasculopathy, pulmonary veno-occlusive disease (PVOD), and lymphatic disorders.

Studies reporting the diagnostic imaging findings for specific forms of chILD in this classification scheme are emerging. In some diseases, such as NEHI and bronchiolitis obliterans, the imaging findings are specific or highly suggestive of the diagnosis, while the imaging findings are entirely nonspecific in others. In any case, the effectiveness of diagnostic imaging depends on the nature and quality of the images obtained.

Imaging Technique

Chest radiographs (CXRs) are commonly performed on a child presenting with symptoms or signs of interstitial lung disease. CXRs have a favorable profile in terms of low radiation dose, low cost, ease of performance, and ready availability, but have limited low-contrast resolution and are very nonspecific. CXRs are usually abnormal in children with interstitial lung disease, with the most common abnormality being hyperinflation. However, a normal CXR does not exclude chILD.[3]

Following its introduction in the 1980s, high-resolution computed tomography (HRCT) quickly became the preferred imaging technique for evaluating the lungs. Compared with CXR, HRCT is more sensitive for detecting chILD, more

Department of Radiology, Baylor College of Medicine, Singleton Department of Diagnostic Imaging, Texas Children's Hospital, Houston, Texas.

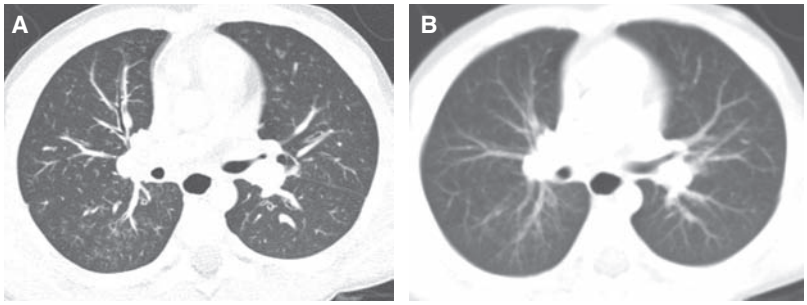

FIG. 1. Fine anatomic details of the lungs are much better depicted on a thin (1.25 mm) axial image slice (**A**) from an HRCT exam than on a thicker (5 mm) axial image slice (**B**) from a routine chest CT exam obtained at the same level.

precise for defining disease extent, and more accurate for characterizing disease involvement as interstitial, airspace, or airway.[4] HRCT can detect chILD that is occult on CXR, confirm the presence of chILD when the CXR is abnormal, and facilitate a more refined differential diagnosis compared with CXR.

In conventional HRCT, noncontiguous thin-section (~1 mm thickness) axial images of the lungs are acquired without intravascular contrast and reconstructed with a high spatial resolution algorithm to depict fine details of the lung parenchyma (Fig. 1). The patient is sequentially moved and stopped in the CT scanner to separately acquire each of the image slices at the specified locations or spacing increments (usually 5–20 mm). This technique was developed in an era when the long-imaging times and high radiation doses associated with acquiring thin-section axial images through the entire lungs with the available single-slice step-and-shoot CT technology was prohibitive. Due to the noncontiguous nature of the image slices acquired with conventional HRCT, multiplanar (coronal or sagittal) image reconstructions cannot be generated and there is a risk of missing pulmonary abnormalities located in the gaps between the axial slices, leading to false-negative exams or underestimation of disease extent.[5] The noncontiguous nature of the images also limits assessment of the mediastinum and central airways.[6] Evaluation of the mediastinal and hilar structures on HRCT is further limited by the lack of intravascular contrast.

The advent of multislice helical CT scanners allowed multiple contiguous sections of the lungs to be imaged simultaneously as a volume while the patient is continuously moved through the scanner, dramatically reducing the imaging time (Fig. 2). High-resolution thin-section images of similar quality to conventional HRCT images can be reconstructed from the volumetric data acquired by contemporary multislice helical CT scanners[7] (Fig. 3). If high-resolution thin-section images of the lungs are reconstructed from a multislice helical CT exam, it is very unlikely that the addition of a conventional HRCT will provide further useful information.[8]

Because there is heightened concern of the risks of radiation to children and the radiation dose from a conventional HRCT scan with noncontiguous slices is substantially lower than from a multislice helical CT exam, conventional HRCT is still the generally preferred method of surveying known or suspected diffuse disease of the pulmonary interstitium, peripheral airspaces, or small airways in children.[5,9] Possible exceptions include settings in which pulmonary nodules or bronchiectasis is a primary concern. Multislice helical CT with oblique coronal image reconstructions is more accurate than conventional noncontiguous HRCT for the diagnosis of bronchiectasis, particularly of the right middle lobe and lingula.[10,11] It is important not to confuse blurred pulmonary vessels from motion as bronchiectasis. This is a particularly common artifact adjacent to the heart (Fig. 4).

High-quality CT images of the lungs are essential for evaluating chILD.[12] Factors influencing the quality of CT images of the lungs include patient motion, lung volumes, and CT scanning and image reconstruction technique. Most cases of chILD are diagnosed in infancy or early childhood, the period of life when obtaining high-quality CT images of the lungs is the most difficult due to the small size of the anatomic structures, the rapid respiration of the patient, and the inability of the patient to breath-hold or refrain from moving. Both normal anatomy and lung pathology can be obscured by image blurring from respiratory motion.[13] Technological advances in CT scanner speed have reduced motion artifact and allowed more children to be scanned without sedation. A chest CT can often be successfully performed without sedation on infants up to 6 months of age following normal feeding and swaddling and on cooperative children older

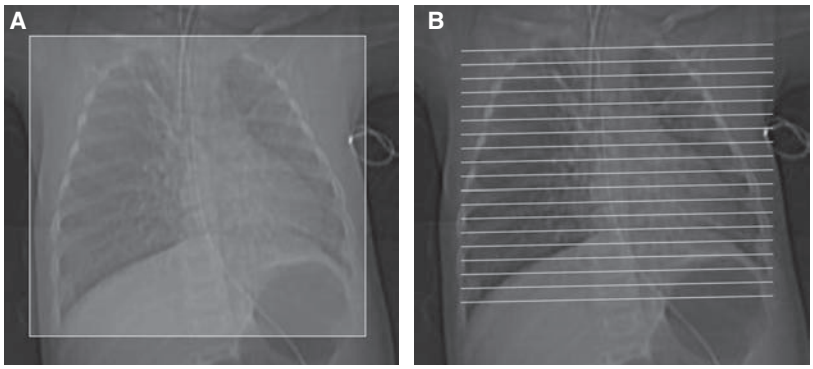

FIG. 2. Volumetric multislice CT technique covers the entire lungs (**A**). Conventional noncontiguous HRCT technique samples only portions of the lungs at increments (**B**), leaving gaps that are not imaged, but exposing the patient to a lower radiation dose.

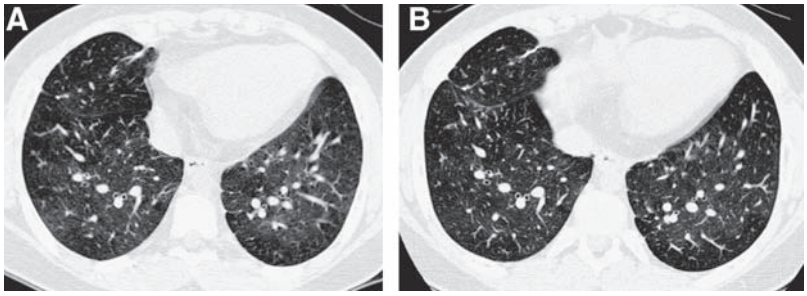

FIG. 3. A thin-section CT image reconstructed from volumetric data acquired by modern multislice helical CT technique (**A**) is very similar in quality to an image acquired by conventional noncontiguous HRCT technique (**B**).

than 3 years of age.[3,14] However, CT scanners are still not fast enough to acquire motion-free images of the lungs in patients incapable of breath-holding.[15]

HRCT exams should generally include a set of images acquired after deep inspiration with the lung volumes near total lung capacity. The greater the lung inflation, the greater the inherent contrast between air and the lung soft tissues, the lower the radiation dose necessary to resolve the lung soft tissues, the greater the conspicuity of the airways, the lesser the atelectasis, the higher the sensitivity for bronchiectasis, and the more reproducible the images are for follow-up[6] (Fig. 5). The greater the spacing increment between the noncontiguous HRCT images, the lower the radiation dose but the greater the undersampling of lung tissue, and a spacing increment of >10 mm for the inspiratory images may compromise evaluation of lung disease that is diffuse but heterogeneous in distribution.[16] A set of expiratory HRCT images of the lungs with the lung volumes at or below functional residual capacity should be acquired if a disorder with pulmonary air trapping or airway malacia is a clinical concern. An expiratory state of the lungs on HRCT images is suggested if the posterior tracheal membrane is horizontal or concave, while a convex contour suggests an inspiratory state (Fig. 6). Expiratory HRCT images can be obtained at greater increments than the inspiratory images to minimize the radiation dose, but a sampling density below 6% of the whole lung significantly decreases the precision of evaluation of air trapping.[17]

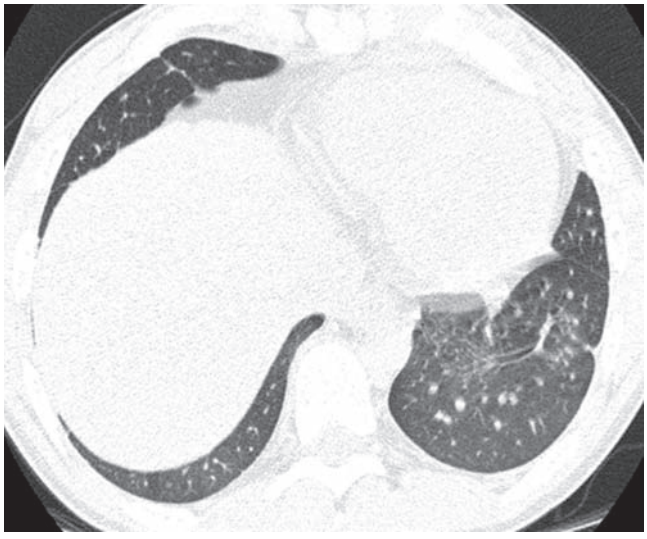

FIG. 4. Blurring of pulmonary vessels from motion induced by transmitted cardiac pulsations can obscure or simulate pathology such as bronchiectasis on CT, particularly in the lower left lung adjacent to the heart.

Images of the lungs obtained during quiet respiration at shallow tidal volumes are less sensitive for bronchiectasis and air trapping and are compromised by motion artifact and pulmonary underexpansion that can mask or mimic pathology, possibly leading to an unnecessary or misdirected lung biopsy[12,13] (Fig. 7). Infants and young children typically cannot cooperate with breath-hold maneuvers necessary for obtaining high-quality HRCT images of the lungs. School-age children can usually comply with instructions for breath-holding near full lung inflation after deep inspiration, but compliance with expiratory breath-hold instructions is difficult to achieve even in older children, and often requires diligent coaching and practice prior to the CT scan.

When volitional breath-holding by the patient is not feasible, options for acquiring inspiratory and expiratory HRCT images of the lungs include decubitus positioning of the patient, respiratory-gated or dynamic cine CT, and controlled-ventilation CT under sedation or general anesthesia. In decubitus positioning, the volume of the dependent lung is similar to that in an expiratory state and the volume of the nondependent lung is similar to that in an inspiratory state.[18] Disadvantages of decubitus positioning include slice misregistration and arousing the patient from a sedated state. Respiratory-gated CT allows precise timing of image acquisition with phases of the respiratory cycle during free breathing, but requires special equipment that may not be available at many institutions. The very fast image acquisition times possible with modern CT scanners allows multiple cine CT images of a lung section or airway to be obtained throughout the respiratory cycle, dynamically revealing air trapping or airway malacia during expiration.[19]

General anesthesia with endotracheal tube or laryngeal mask airway ventilation is an effective method for obtaining motion-free inspiratory and expiratory images, but is invasive, expensive, and subject to procedural risks.[13] Infants and children are particularly prone to atelectasis under general anesthesia due to their high chest wall compliance and underdeveloped collateral ventilation system (pores of Kohn and channels of Lambert) coupled with the loss of respiratory drive and loss of intercostals muscle tone. The lung CT images obtained from infants and children under general anesthesia are often compromised by atelectasis unless

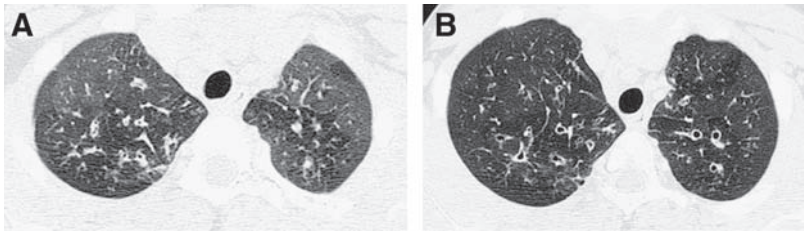

FIG. 5. The fuller the lung inflation the greater the distention of the airways; consequently, bronchiectasis that is occult on HRCT performed at low lung volumes (**A**) may become overt on HRCT performed at deep inspiration (**B**).

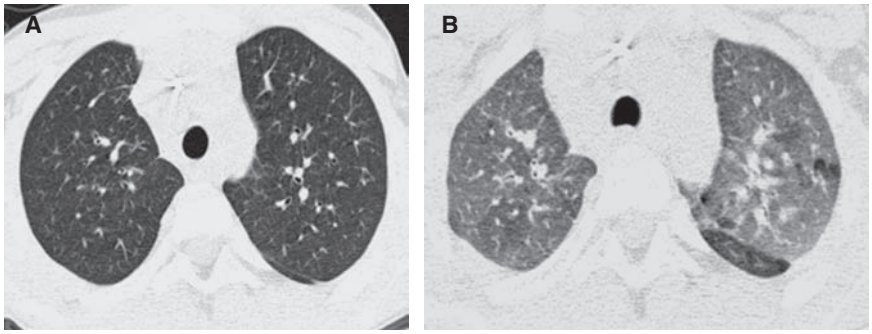

FIG. 6. Compared with its appearance on inspiratory HRCT (**A**), the normal lung manifests increased attenuation on expiratory HRCT (**B**) due to the lower proportion of air relative to solid pulmonary parenchymal tissue at smaller lung volumes. An inspiratory state is suggested by a convex contour of the posterior tracheal membrane, while a horizontal or concave contour of the posterior tracheal membrane suggests an expiratory state.

alveolar recruitment maneuvers with adequate positive inspiratory and end-expiratory pressures are used and scanning is performed promptly after anesthesia induction.[20] Imaging the lung regions of concern with the patient in both supine and prone positions can be used to re-expand dependent atelectasis (Fig. 8) and to clarify the nature of dependent lung opacities (Fig. 9).

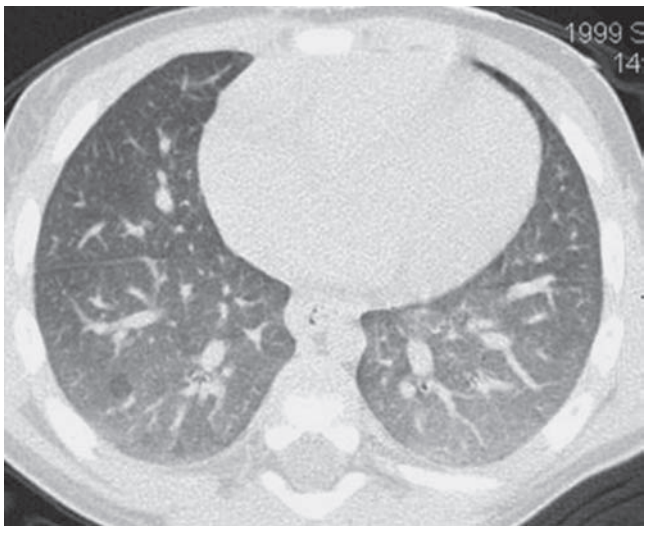

FIG. 7. A ground-glass appearance with hazy increased attenuation of the lungs and preserved visibility of the bronchovascular structures can occur physiologically on a chest CT image obtained at tidal volumes during quiet respiration and simulate diffuse lung disease. This physiologic increase in lung attenuation is more pronounced dependently where the pulmonary vascular blood volume is greatest and the airspaces are least distended (image courtesy of Fred Long, M.D.).

As an alternative to general anesthesia and intubation, transient respiratory pauses long enough to acquire motion-free CT images of the lungs can be induced in a sedated infant or young child by synchronously applying positive pressure with face-mask ventilation to several consecutive spontaneous tidal inspirations. The lungs can be inflated with sustained positive pressure or allowed to deflate during the respiratory pause to acquire CT images at desired lung volumes. This controlled-ventilation CT technique requires coordination with an anesthesiologist or respiratory therapist familiar with the required ventilator maneuvers, and the respiratory pause may not be of adequate length for expiratory imaging if the child is very tachypneic.[21]

The method of CT image reconstruction also influences image quality. HRCT images of the lungs are usually reconstructed at a slice thickness of ~1 mm. Finer structures can be resolved with thinner slices but at the cost of increased image noise unless the radiation dose used to acquire the images is increased. The image reconstruction algorithm that provides the best spatial resolution at a tolerable image noise level is generally preferred for HRCT and is dependent on the proprietary techniques that vary among CT scanner models. HRCT images of the lungs generated with so-called "bone" reconstruction algorithms may be preferable to those generated with "lung" reconstruction algorithms due to edge enhancement effects with the latter that can result in overestimation of the extent of diffuse lung disease[22] (Fig. 10). The appearance of the lung parenchyma and airways is also influenced by the windowing selected for image display. A window width of around 1,500 HU (Hounsfield units) is usually selected for HRCT image viewing, and too wide of a window width can obscure mosaic attenuation, cysts, and air trapping, while too narrow of a window width can result in artifactual ground-glass opacification or artifactual bronchial wall thickening (Fig. 11).

Radiation exposure to children from CT exams is an increasing concern. Depending on technique, the radiation dose from a chest CT can range from tens to hundreds of times greater than that from a CXR. Image quality is improved by the use of higher radiation doses, but the goal should be to incur the lowest radiation dose necessary to acquire images of sufficient quality for diagnostic purposes according to the ALARA (As Low As Reasonably Achievable) principle (Fig. 12). CT exams should be performed only in the setting of a clear clinical indication, and the CT imaging technique should be tailored to the clinical indication and patient size, since less radiation is needed to achieve the same image quality in smaller patients. The inherent high contrast between air and lung soft tissues, the small size of children, and the diffuse nature of chILD allow CT images sufficient for the evaluation of chILD to be acquired at relatively low radiation doses. A diagnostic quality helical multislice CT scan of the pediatric chest can be performed with

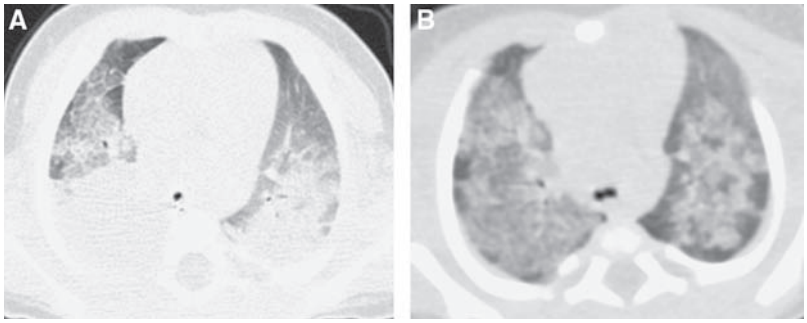

FIG. 8. A CT image shows confluent opacification of the dependent posterior aspects of the lungs of an infant scanned while supine (**A**). A CT image acquired after prone repositioning of the patient (**B**) re-expands the posterior atelectasis and reveals underlying patchy pulmonary consolidation and ground-glass opacification related to surfactant dysfunction from an *SP-C* gene mutation.

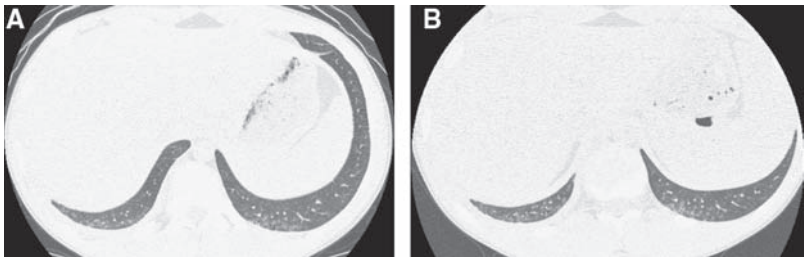

FIG. 9. A supine chest CT image from a teenager with systemic sclerosis image shows peripheral opacities at the dependent posterobasilar lower lobes (**A**). A CT image acquired after prone repositioning of the patient reveals persistence of these opacities which represent pulmonary involvement by systemic sclerosis rather than just atelectasis (**B**).

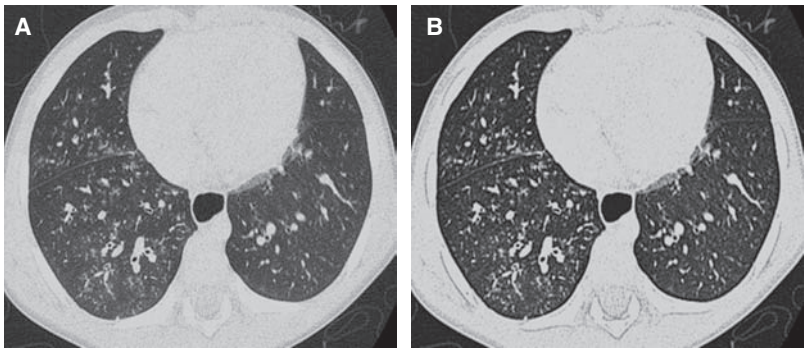

FIG. 10. An HRCT image generated with a "bone" reconstruction algorithm (**A**) is preferable to an HRCT image generated with a "lung" reconstruction algorithm (**B**) due to excessive edge enhancement artifact with the latter, exemplified by the dark etching at the lung periphery.

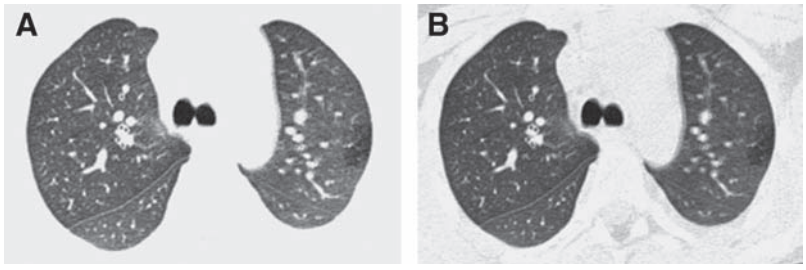

FIG. 11. A hypoattenuating focus of air trapping at the peripheral lateral left upper lobe is more conspicuous on an HRCT image viewed with a narrow (900 HU) window width (**A**) than with a conventional (1,500 HU) window width (**B**), but the narrow window width produces artifactual bronchial wall thickening.

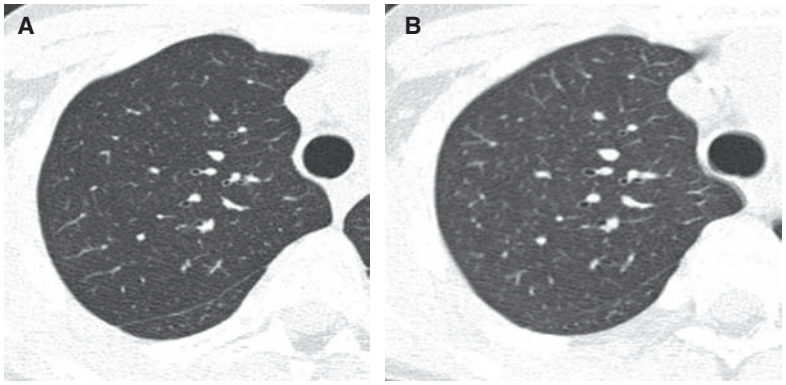

FIG. 12. There is no clinically relevant difference in the diagnostic quality of this HRCT image (**A**) compared with an HRCT image obtained with a 3 times greater radiation dose (**B**). The inherent high contrast between air and lung soft tissues permits HRCT images of diagnostic quality to be acquired with relatively low radiation doses, particularly if the lungs are well inflated.

FIG. 13. Image from an infant HRCT obtained with an estimated radiation effective dose of 0.1 milliSievert, which is equivalent to the dose from a few chest radiographs (CXRs). Although the image quality is degraded by the high noise level, the pattern of ground-glass opacities is sufficiently depicted to corroborate the clinical diagnosis of neuroendocrine cell hyperplasia of infancy.

a radiation dose substantially less than the average annual natural background radiation effective dose of 2–3 milliSievert.[23] By using noncontiguous technique for HRCT, the radiation dose can be reduced to as low as that associated with a few weeks of natural background radiation or a few CXRs and still make a confident diagnosis of certain forms of chILD[24] (Fig. 13).

Magnetic resonance imaging (MRI) is a good modality for assessing the mediastinum and chest wall and does not entail exposure of the patient to ionizing radiation. However, conventional MRI is of limited utility for evaluating chILD due to the low proton content of the lungs and poor depiction of the pulmonary interstitium. Specialized MRI using inhaled hyperpolarized gases as a contrast agent has shown promise as an investigational technique for imaging the pulmonary airspaces. Measuring the diffusion of hyperpolarized gas in the pulmonary airspaces with MRI provides information on alveolar morphology and could be used as a noninvasive means to identify children with lung growth disorders characterized by enlarged simplified alveoli.[25]

Imaging Findings in ChILD

Correct interpretation of chest imaging studies in children requires high-quality images so that abnormalities can be confidently identified and characterized.[5] A properly performed HRCT can depict the pulmonary airways and vessels down to the level of the secondary pulmonary lobule, the smallest lung unit demarcated by connective tissue septations. Centrilobular arteries (1 mm diameter) are visible by HRCT, but intralobular bronchioles and alveoli (<0.2 mm diameter) are normally too small to resolve.[26] Interlobular septa can occasionally be seen by CT in the normal lung, especially at the periphery of the anterior, lateral, and juxtamediastinal regions of the upper and middle lobes, and at the periphery of the anterior and juxtadiaphragmatic regions of the lower lobes.[27] Because of the resolution limits, HRCT cannot truly distinguish alveolar spaces from the interstitium, and diffuse lung disease is a more appropriate descriptor than interstitial lung disease.

To effectively describe and communicate findings on HRCT, application of a standardized lexicon is advised. Terminology such as "ground-glass," "tree-in-bud," "crazy-paving," and "honeycombing" should be used in accordance with the precise definitions provided by the glossary of terms for thoracic imaging from the Fleischner Society.[28] Potentially confusing descriptors should be avoided. For example, the presence of nonspecific findings does not warrant an interpretation of nonspecific interstitial pneumonia (NSIP), which is actually a specific clinicopathologic diagnosis.

Pulmonary abnormalities found on HRCT in chILD predominantly consist of some combination of hyperinflation, mosaic attenuation, air trapping, ground-glass opacities, consolidation, linear/reticular opacities, nodules, or cysts. A mosaic attenuation pattern in children is usually attributable to patchy interstitial disease or small airway disease with air trapping, but can also be seen with pulmonary hypertension, thromboembolism, or other occlusive vascular diseases that result in mixed oligemic and plethoric lung.[5,14] Air trapping appears on HRCT as hypoattenuating regions that exhibit less than a normal increase in attenuation and less than a normal decrease in volume on expiratory images[28] (Fig. 14). It is not unusual to see a few subsegmental hypoattenuating foci in the lungs of normal children, especially in the posterior juxtapleural region.

In consolidation, the airspace opacification obscures the pulmonary vessels (Fig. 15). Consolidation can be seen in

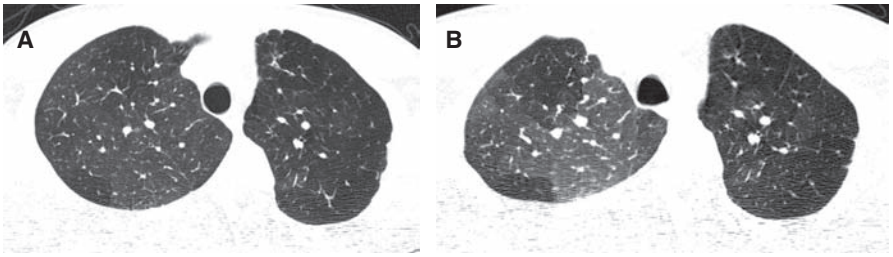

FIG. 14. Inspiratory (**A**) and expiratory (**B**) HRCT images of a patient with bronchiolitis obliterans show mosaic attenuation of the lungs with patchy ground-glass opacification that is accentuated on expiration. Areas of pulmonary air trapping related to obliterated airways exhibit decreased conspicuity of the pulmonary vessels, little decrease in volume on expiration, and little increase in attenuation on expiration. Areas of spared normal lung exhibit marked increased attenuation on expiration related to the decreased volume of air in the airspaces and the increased capillary blood flow diverted from the areas with air trapping.

infectious pneumonia, organizing pneumonia, eosinophilic pneumonia, aspiration pneumonia, acute interstitial pneumonia (AIP), pulmonary hemorrhage syndromes, and alveolar pulmonary edema.[27] Ground-glass opacity is defined as hazy increased attenuation of the lung with preserved visibility of the bronchovascular structures on HRCT. Ground-glass opacity is very nonspecific and can be seen in lung with increased capillary blood volume, such as from shunting, or in lung affected by processes that thicken the interstitium or partially remove or replace the air in the alveoli with cells, fluid, or other material[5,27,29] (Figs. 8, 13, and 14). Ground-glass opacities can also be observed physiologically in underinflated lungs, particularly in the dependent lung bases of infants on images acquired at expiration or shallow inspiration[30] (Fig. 7).

Interlobular or intralobular septal thickening results from edematous, infiltrative, or fibrotic processes affecting the pulmonary interstitium and produces a linear or reticular pattern on HRCT. The septal thickening is typically smooth in cases of pulmonary edema, lymphangiectasis, and lymphangiomatosis (Fig. 16), and nodular in cases of sarcoidosis and lymphoid interstitial pneumonia (LIP). A fine pattern of linear or reticular septal thickening can be seen in NSIP and connective tissue disorders (Fig. 17), and a coarse pattern with subpleural bands and architectural distortion suggests fibrosis[27,29] (Fig. 18). Crazy-paving refers to the pattern of septal thickening superimposed on a background of ground-glass opacity, evocative of the appearance of irregularly shaped paving stones[28] (Fig. 19). Crazy-paving is associated with pulmonary alveolar proteinosis (PAP), pulmonary hemorrhage syndromes, exogenous lipoid pneumonia, DAD, organizing pneumonia, *Pneumocystis* pneumonia, and idiopathic pneumonia syndrome.

Pulmonary nodules can be classified according to their distribution as perilymphatic, military, or centrilobular. Perilymphatic nodules are found along the interlobular septa, interlobar fissures, and bronchovascular bundles, and may be seen in sarcoidosis (Fig. 20). Miliary nodules have a random distribution indicating hematogenous dissemination, and may be seen in miliary tuberculosis, metastatic disease, and Langerhans cell histiocytosis (LCH) (Fig. 21). Centrilobular nodules are found within the secondary pulmonary lobule and are separated from the pleural fissures and interlobular septa by a distance of several millimeters.

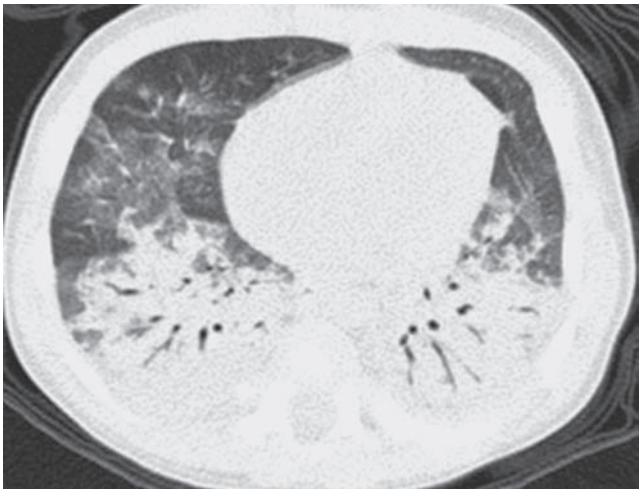

FIG. 15. Chest CT image from a case of aspiration pneumonia showing consolidation with air bronchograms involving the lower lobes of the lungs.

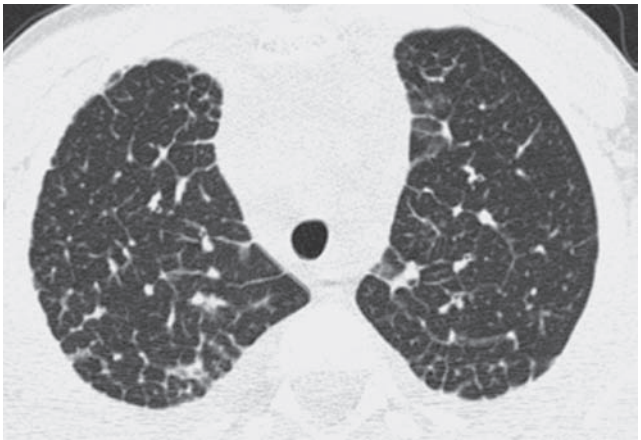

FIG. 16. HRCT in a patient with lymphangiomatosis shows linear and polygonal opacities related to interlobular septal thickening, most conspicuously at the peripheral paramediastinal and posterior lung regions.

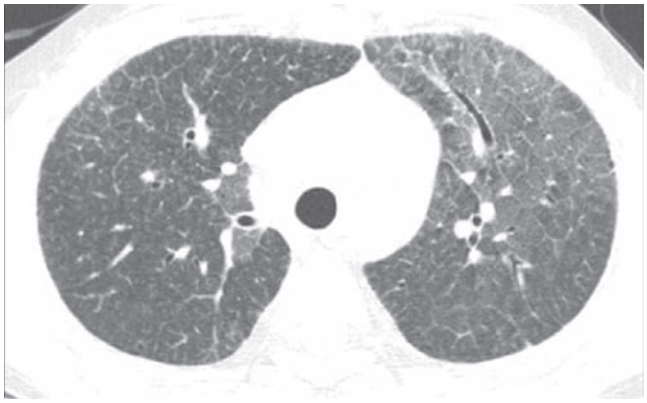

FIG. 17. A fine reticular pattern of septal thickening is demonstrated on this HRCT image from a child with nonspecific interstitial pneumonia.

Centrilobular nodules are often ill-defined and ground-glass in attenuation, and are commonly seen in hypersensitivity pneumonitis, bronchiolitis, cystic fibrosis, asthma, immotile cilia syndrome, idiopathic pulmonary hemosiderosis (IPH), and PVOD[14,27] (Fig. 22). The tree-in-bud pattern refers to branching centrilobular opacities that resemble a budding tree, and is most commonly observed in disorders associated with endobronchiolar plugging, such as cystic fibrosis and bronchiolitis (Fig. 23), but can also be seen in diseases such as capillaritis that affect the intralobular vessels.[28]

A cyst appears on CT as a round low-attenuating structure with a well-defined interface with normal lung. Cysts usually contain air but occasionally contain fluid or solid material.[28] Thin-walled cysts are seen in pulmonary LCH, LIP, NSIP, lung growth disorders, disorders of surfactant metabolism, and pulmonary alveolar microlithiasis (Fig. 24). Thicker-walled cysts seen in honeycombing reflect the dissolution of alveoli and loss of acinar architecture associated with pulmonary fibrosis.

FIG. 19. HRCT image from a patient with acute myelogenous leukemia and idiopathic pneumonia syndrome shows a "crazy-paving" pattern of superimposed septal thickening and ground-glass opacification, most conspicuously in the right lung.

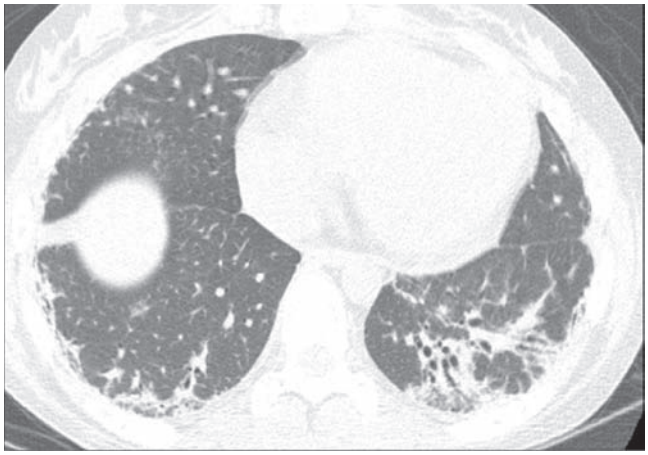

FIG. 18. A chest CT image from a patient with juvenile dermatomyositis shows coarse peripheral opacities with subpleural bands, architectural distortion, and traction bronchiectasis related to pulmonary fibrosis.

Imaging Features of Specific Disorders

While rare, the disorders comprising chILD are likely under-recognized on imaging studies. Chest imaging studies on children are frequently performed at institutions without pediatric thoracic radiology expertise and the studies are often interpreted by those unfamiliar with newly characterized disorders and reclassifications of previous disorders. To serve as a guide for those interpreting pediatric chest imaging studies, the following section will review the salient imaging features of specific disorders in the chILD spectrum, focusing initially on the disorders that typically present in infancy, followed by the disorders that are primarily encountered later in childhood. Knowledge of the imaging findings in chILD is predominantly derived from descriptive case reports and small retrospective cross-sectional case series. Larger prospective and longitudinal studies are still needed to demonstrate the natural evolution of the findings with aging and growth, and to define the diagnostic performance characteristics of imaging in terms of its sensitivity,

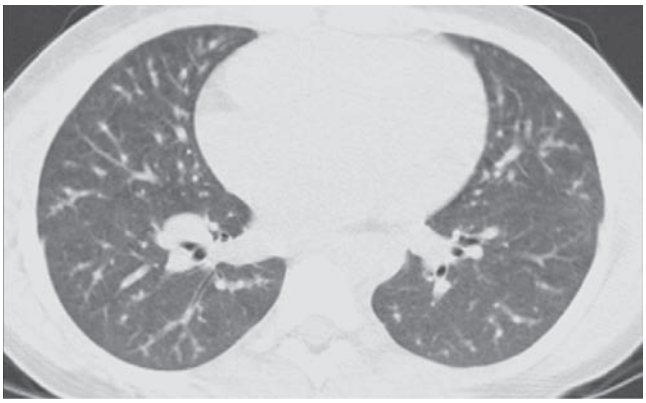

FIG. 20. The presence of perilymphatic nodules gives a beaded appearance to some of the bronchovascular bundles on this chest CT image from a patient with pulmonary sarcoidosis.

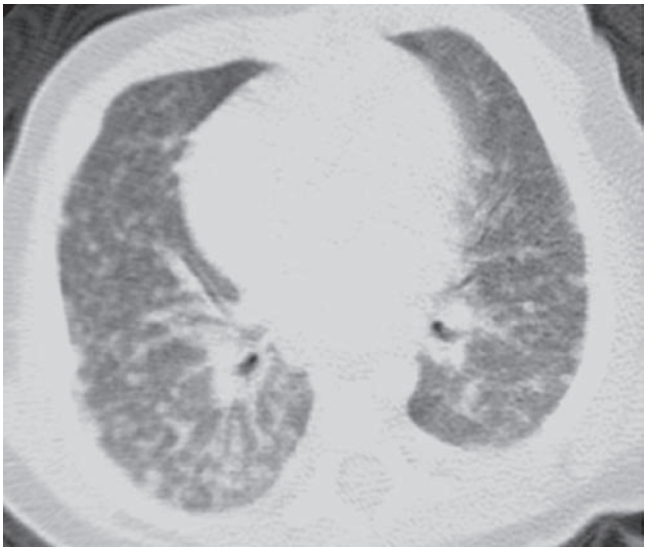

FIG. 21. Hematogenous dissemination of the disease process in miliary tuberculosis is represented by the presence of randomly distributed pulmonary nodules on this chest CT image.

specificity, accuracy, likelihood ratios, and predictive values for specific disorders in the chILD spectrum.

Diffuse Developmental Disorders

The diffuse developmental disorders of the lung include acinar dysplasia, congenital alveolar dysplasia, and alveolar capillary dysplasia with misalignment of pulmonary veins (ACD/MPV). ACD/MPV is associated with forkhead box (*FOX*) gene mutations and deletions and most cases are associated with extrapulmonary abnormalities, including hypoplastic left heart syndrome, urinary tract malformations, and intestinal malrotation and atresias.[31] The usual presentation is a full-term neonate that develops progressive respiratory distress and cyanosis within 48 h of birth.

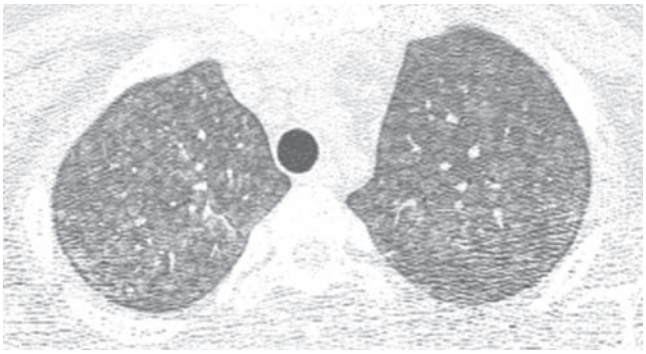

FIG. 22. Numerous centrilobular ground-glass nodular opacities are depicted on this chest CT image from an adolescent with hypersensitivity pneumonitis.

Knowledge of the imaging features of the diffuse developmental disorders is limited to descriptions of the CXRs from case reports and small case series of ACD/MPV and acinar dysplasia. The lungs may be initially clear on CXR, and follow-up radiographs show progressive hazy bilateral pulmonary opacification, similar to that seen with surfactant deficiency of prematurity or inborn errors of surfactant metabolism. Air leaks including pneumothorax and pneumomediastinum develop in 50%, likely from barotrauma[32–34] (Fig. 25). Although the CXR findings are nonspecific, diagnosis should be considered in the setting of a full-term neonate with severe respiratory distress resembling persistent pulmonary hypertension of the newborn but lacking the usual predisposing features such as meconium aspiration, asphyxia, prematurity, or sepsis.[35]

Lung Growth Disorders

The lung growth disorders are characterized by defective alveolarization with lobular simplification, deficient alveolar septation, and airspace enlargement that may be misinterpreted as "emphysematous changes" on imaging and pathologic inspection. Prenatally, the best known form

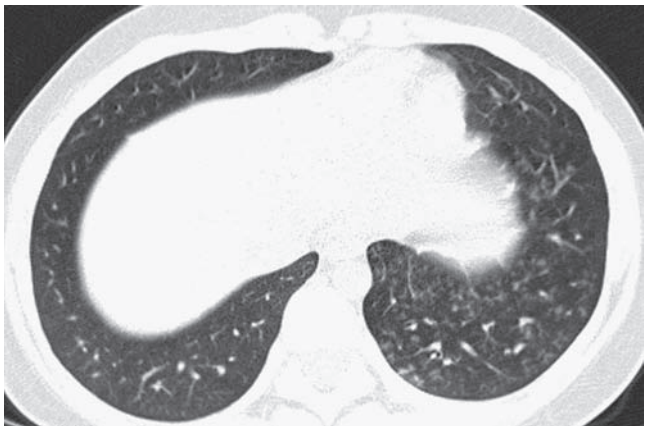

FIG. 23. Branching centrilobular opacities in a tree-in-bud pattern are shown in the left lower lobe on this chest CT image from an adolescent with an atypical mycobacterial infection and lymphocytic bronchiolitis.

FIG. 24. A chest CT image from a child with pulmonary Langerhans cell histiocytosis demonstrates numerous air-filled thin-walled cysts in the lungs.

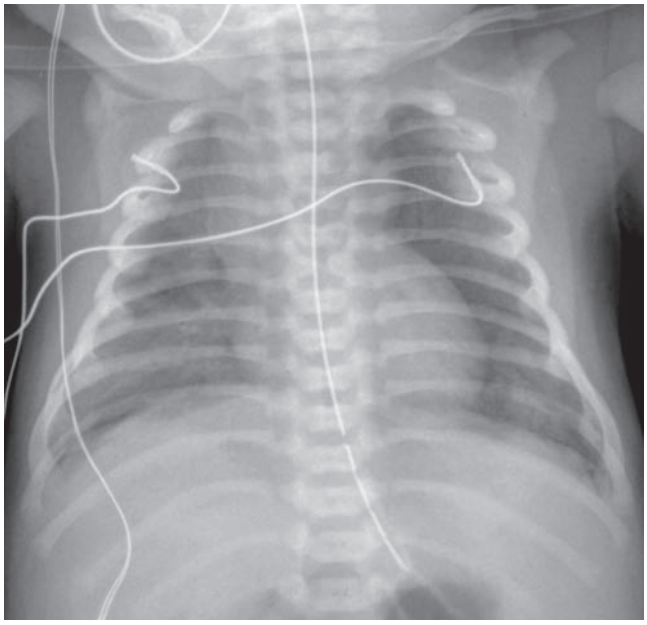

FIG. 25. CXR of a full-term neonate with alveolar capillary dysplasia with misalignment of the pulmonary veins shows hazy pulmonary opacities resembling the findings of surfactant deficiency. Small pneumothoraces and pneumomediastinum related to air leak from barotrauma are also present.

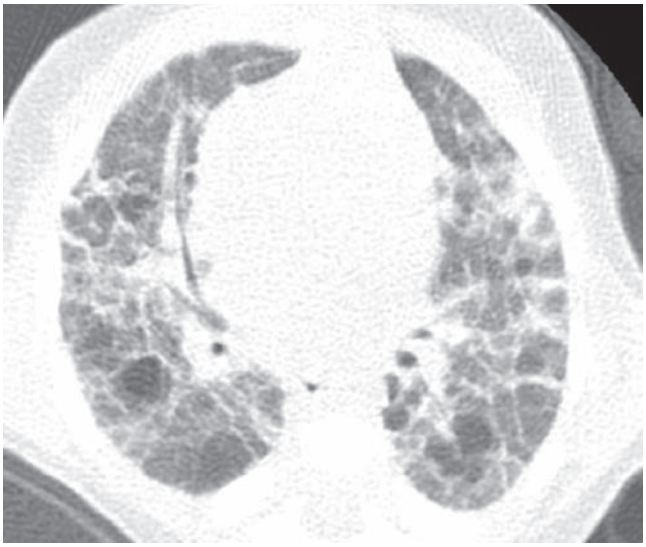

FIG. 26. A chest CT image from a very premature neonate with bronchopulmonary dysplasia exhibits hyperlucent areas that correspond to alveolar enlargement and simplification and reduced distal vascularization, and linear opacities that correspond to interstitial fibroproliferation.

is pulmonary hypoplasia related to oligohydramnios or *in utero* restriction of fetal thoracic space. Postnatally, the most commonly encountered form is chronic neonatal lung disease of prematurity or bronchopulmonary dysplasia (BPD).[2]

BPD is a disorder of lung growth impairment, injury, and repair originally attributed to positive pressure mechanical ventilation and oxygen toxicity. On CXR, infants with classic BPD demonstrate coarse reticular pulmonary opacities, cystic lucencies, and disordered lung aeration reflecting alternating regions of alveolar septal fibrosis and hyperinflated lung parenchyma. Advances in perinatal medicine, including administration of antenatal glucocorticoids, surfactant replacement therapy, and refined ventilatory strategies, have lowered the threshold of viability to ~23 weeks gestational age when the alveolar ducts and alveoli are just beginning to develop. Compared with classic BPD, the "new" BPD is a disorder of extremely premature neonates with arrested or delayed alveolar and pulmonary vascular development, less pronounced alveolar septal fibrosis and inflammation, and more subtle imaging abnormalities.[36] The most frequent abnormalities of new BPD on CT are hyperlucent areas, linear opacities, and triangular subpleural opacities (Fig. 26). The hyperlucent areas correspond to alveolar enlargement and simplification and reduced distal vascularization. The linear and subpleural opacities correspond to interstitial fibroproliferation and are associated with a low functional residual capacity, oxygen supplementation, and mechanical ventilation. The CT findings do not correlate with the severity of current symptoms.[37]

Lung growth disorders with lobular simplification and alveolar enlargement may also be encountered in term infants, often in the setting of congenital heart disease or genetic disorders such as trisomy 21. The Imaging Working Group of the chILD Research Cooperative noted variability in the imaging findings associated with lung growth disorders, including distortion of the lung architecture with perilobular opacities and lobules of variable attenuation on chest CT in some cases[2] (Fig. 27). Subpleural cysts along the lung periphery, pulmonary fissures, and bronchovascular bundles are visible in 36% of children with the lung growth disorder associated with trisomy 21[38] (Fig. 28). Mutations of the filamin A (*FLNA*) X-linked gene are associated with periventricular nodular gray matter heterotopia, cardiovascular anomalies, skeletal dysplasia, Ehlers-Danlos variants, and a lung growth disorder characterized by simplified enlarged alveolar airspaces and pulmonary hypertensive changes leading to progressive respiratory failure in infancy. The chest imaging findings of the lung growth disorder associated with FLNA mutations consist of severe multilobar hyperinflation with hyperlucent lung parenchyma and peripheral pulmonary vascular attenuation resembling emphysema[39] (Fig. 29).

Neuroendocrine Cell Hyperplasia of Infancy

Neuroendocrine cell hyperplasia of infancy (NEHI), originally reported as persistent tachypnea of infancy, typically presents before 2 years of age with tachypnea, hypoxia, and retractions and usually has a prolonged, slowly improving course unresponsive to steroids. HRCT findings of air trapping in a mosaic attenuation pattern affecting at least 4 lobes with geographic ground-glass opacities that are most conspicuous of the right middle lobe and lingula are very characteristic of NEHI (Fig. 30). When interpreted by experienced pediatric thoracic radiologists, the sensitivity and specificity of HRCT for NEHI are 78%–83% and 100%, respectively.[24] Unlike many other forms of chILD, a specific

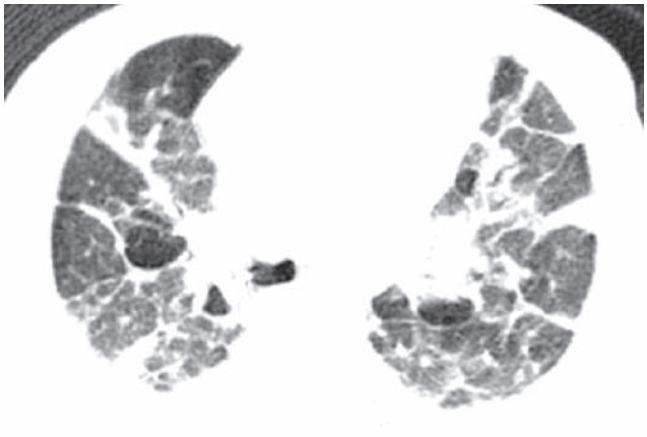

FIG. 27. A chest CT image from a 4-month-old term infant with respiratory insufficiency showing distortion of the lung architecture with perilobular opacities and pulmonary lobules of variable attenuation. Histopathologic inspection revealed a lung growth disorder characterized by lobular simplification and alveolar enlargement.

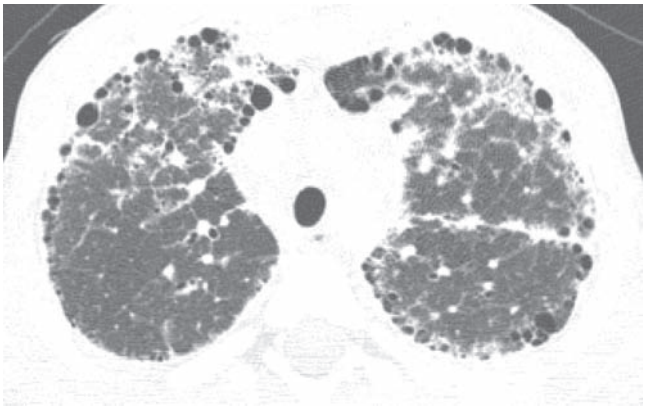

FIG. 28. Multiple subpleural cysts are demonstrated on this chest CT image from a 5-year-old with a lung growth disorder associated with trisomy 21.

diagnosis of NEHI can be suggested by HRCT, and a confirmatory biopsy may not be necessary for patients with a classic clinical presentation and characteristic radiologic findings.[12] However, the diagnosis cannot be excluded by radiographs, and misdiagnoses can occur when other abnormalities such as superimposed infections are present and the distribution pattern of ground-glass opacities is atypical.[24] CXRs consistently show hyperexpansion, which can be confused for reactive airways disease or bronchiolitis in infants[40] (Fig. 31). Most patients require supplemental oxygen for many years and hyperinflation may persist into adolescence.[41]

Pulmonary Interstitial Glycogenosis

Pulmonary interstitial glycogenosis (PIG), also known as neonatal pulmonary interstitial glycogen accumulation disorder and infantile cellular interstitial pneumonitis, typically presents with respiratory distress in the early neonatal period and is characterized by interstitial thickening with immature glycogen-laden mesenchymal cells without inflammation or fibrosis. The radiographic abnormalities are nonspecific. CXR shows progressive hyperinflation and evolution from a fine interstitial to a coarse interstitial and alveolar pattern. HRCT demonstrates distortion of the lung architecture with linear and ground-glass opacities mixed with hyperinflated or hyperlucent areas. There is often clinical, histologic, and radiologic amelioration over the first few

FIG. 29. An HRCT image from an infant with a filamin A gene mutation shows severe multilobar pulmonary hyperinflation and hyperlucency with peripheral pulmonary vascular attenuation resembling emphysema. A lung growth disorder characterized by simplified enlarged alveolar airspaces and pulmonary hypertensive changes was noted on a lung biopsy specimen.

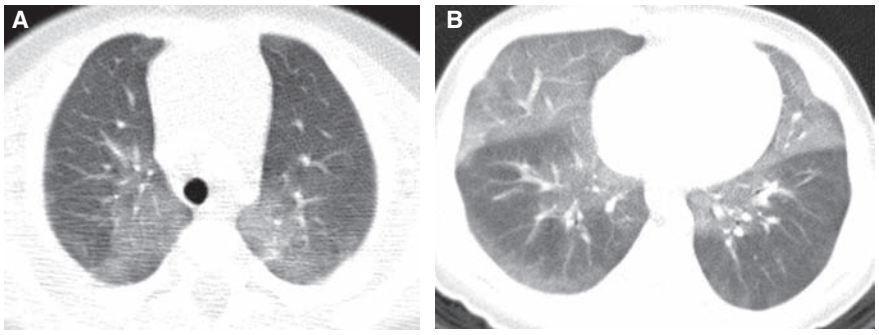

FIG. 30. Chest CT images of a 3-month-old infant with persistent tachypnea show mosaic attenuation with geographic ground-glass opacities of the posteromedial upper lobes (**A**), infrahilar lower lobes, right middle lobe, and lingula (**B**). These findings are highly characteristic of neuroendocrine cell hyperplasia of infancy.

months of life, but hyperexpansion of the lungs may persist for years.[42–45] PIG can be an isolated disorder, but is more commonly seen as a patchy process in infants with lung growth disorders, and the radiographic findings and clinical course in these cases tend to be dominated by the severity of the lung growth disorder[2] (Fig. 32).

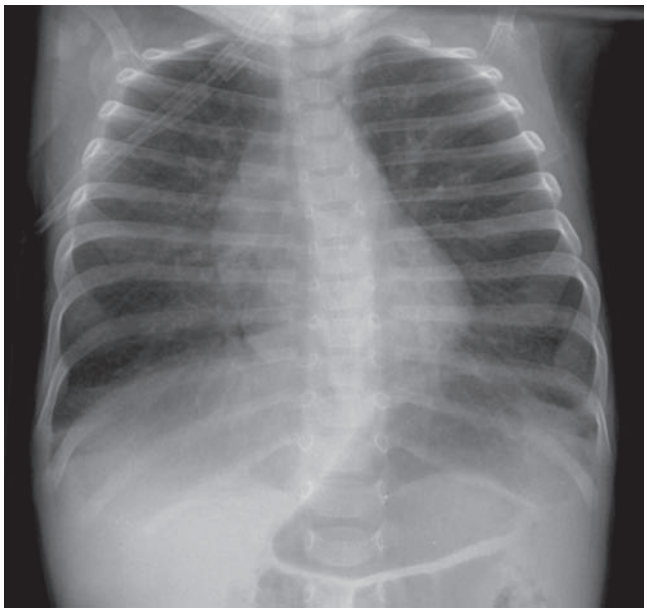

FIG. 31. The CXR of a 9-month-old infant with neuroendocrine cell hyperplasia of infancy shows pulmonary hyperexpansion. This can be misattributed to reactive airways disease or bronchiolitis.

Inborn Errors of Surfactant Metabolism

The importance of a developmental perspective on chILD is illustrated by the different histopathologic patterns manifested by the inborn errors of surfactant metabolism at different ages. Histopathologies associated with inborn errors of surfactant metabolism include chronic pneumonitis of infancy, PAP, desquamative interstitial pneumonia, endogenous lipoid pneumonia, and NSIP. The clinical and radiologic manifestations correspondingly vary with patient age, suggesting the influence of environmental factors and other genes.[46]

Term neonates with homozygous loss-of-function mutations of the surfactant protein B (*SP-B*) gene usually develop diffuse lung disease resembling respiratory distress syndrome (RDS) of surfactant-deficient premature infants, but are refractory to treatment for RDS and succumb to their disease unless lung transplantation is performed. CXR shows diffuse granular or hazy pulmonary opacities, while HRCT shows diffuse ground-glass opacities, interlobular septal thickening, and crazy-paving.[47,48] The differential diagnosis includes infection, obstructed pulmonary venous return, and diffuse developmental disorders.

In term infants, autosomal dominant mutations of the surfactant protein C (*SP-C*) gene or autosomal recessive mutations of the ATP-binding cassette subfamily A member 3 (*ABCA3*) gene can be associated with respiratory failure similar to that seen with *SP-B* mutations, with diffuse hazy pulmonary airspace opacification on CXR and diffuse

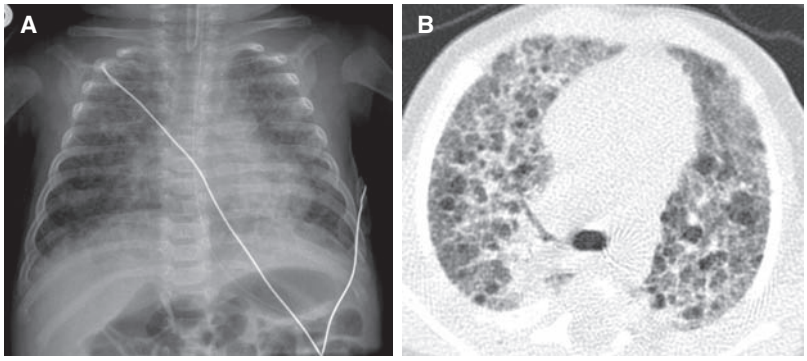

FIG. 32. The CXR (**A**) of a 2-month-old former premature infant with a persisting supplemental oxygen requirement shows a coarse interstitial pattern, while HRCT (**B**) demonstrates distortion of the lung architecture with ground-glass opacities and pulmonary lobules of variable attenuation. Lung biopsy revealed patchy pulmonary interstitial glycogenosis superimposed on a severe lung growth disorder.

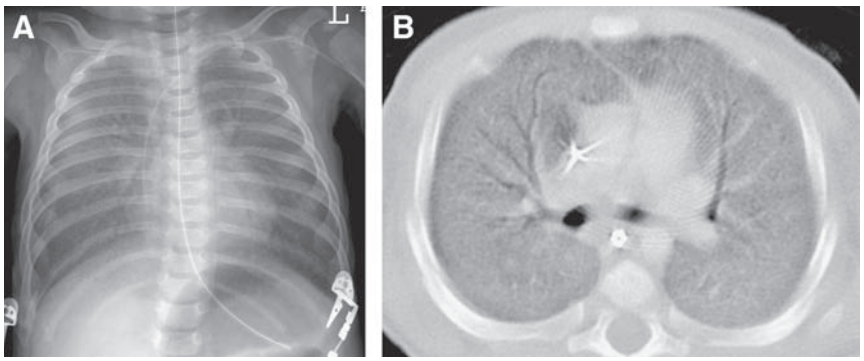

FIG. 33. A full-term infant with respiratory failure related to *ABCA3* gene mutations exhibits diffuse hazy granular pulmonary airspace opacification on CXR (**A**) resembling the findings of surfactant deficiency of prematurity. Diffuse ground-glass pulmonary opacification is observed on chest CT (**B**).

ground-glass opacities, interlobular septal thickening, and crazy-paving on CT[49,50] (Fig. 33). *ABCA3* and *SP-C* gene mutations can also be associated with chronic interstitial lung disease presenting later in infancy and childhood.[51,52] In these older patients, the ground-glass opacities can be diffuse or patchy and the septal thickening can be fine or coarse with architectural distortion. Small pulmonary cysts develop and increase in number and size over time. Pectus excavatum also develops in those surviving beyond infancy[52] (Fig. 34).

When the above imaging findings are noted in a neonate with unexplained or refractory RDS or in an older infant or child with unexplained respiratory insufficiency, particularly if familial, genetic testing for surfactant gene mutations should be pursued and could avert the need for lung biopsy in some cases.[46,48] Routine imaging surveillance is not warranted following diagnosis since changes in the imaging findings do not correlate with lung function or outcome.[52]

Pulmonary Alveolar Proteinosis

Pulmonary alveolar proteinosis (PAP) is characterized by intra-alveolar accumulation of lipoproteinaceous material. The congenital form of PAP presenting in the neonatal period is usually caused by inborn errors of surfactant metabolism. The idiopathic form of PAP is more insidious, presenting later in childhood or adulthood, and is now known to be most commonly related to the presence of neutralizing autoantibodies to granulocyte macrophage colony-stimulating factor (GM-CSF) that disrupts signaling of alveolar macrophages, resulting in impaired clearance of surfactant-derived intra-alveolar lipoproteins, but preserving the underlying lung architecture. Secondary PAP is associated with leukemia, inhalation of toxic fumes or dusts, or other processes that inhibit alveolar macrophage function.[53] Very rare defects of the GM-CSF receptor α or β subunit gene, solute carrier family 7 subfamily A isoform 7 (*SLC7A7*) gene, NK2 homeobox 1(*NKX2-1*)/(thyroid transcription factor 1 (*TTF-1*) gene, or Niemann–Pick disease type C2 (*NPC2*) gene can also lead to PAP in infancy or childhood. *SLC7A7* mutations are associated with lysinuric protein intolerance; *NPC2* mutations are associated with hepatosplenomegaly and Niemann–Pick disease type C2[54]; and *NKX2-1/TTF-1* mutations are associated with concomitant maldevelopment of the basal ganglia and thyroid.[55]

The CXR pattern of PAP is diffuse or perihilar airspace opacification. HRCT tends to show widespread ground-glass opacities, consolidation, septal thickening, and crazy-paving[56–60] (Fig. 35). In the case of autosomal recessive lysinuric protein intolerance due to *SLC747* gene mutations, HRCT can show PAP prior to clinical symptoms and facilitate early diagnosis.[61,62] Opportunistic infections (especially *Pneumocystis jiroveci*, *Listeria monocytogenes*, *Mycobacterium tuberculosis*, adenovirus, and group B streptococcus) are an important source of morbidity and mortality in PAP patients, and can be difficult to diagnose radiographically in the setting of underlying widespread pulmonary disease.

Pulmonary Lymphangiectasia and Lymphangiomatosis

Pulmonary lymphangiectasia is characterized by dilation of the lymphatics draining the subpleural and pulmonary interstitial spaces. The primary form can be restricted to the lungs or can be generalized and involve extrapulmonary structures. The secondary form is due to pulmonary lymphatic or venous

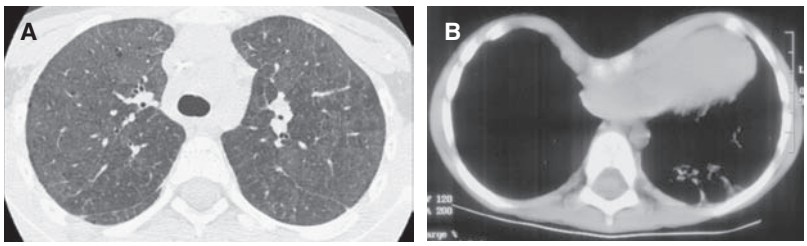

FIG. 34. HRCT image (**A**) of a 10-year-old with cough and dyspnea shows extensive ground-glass pulmonary opacities, small cysts, and a few thickened septa. Additional evaluation revealed *ABCA3* gene mutations, demonstrating that inborn errors of surfactant metabolism can present after infancy with chronic diffuse lung disease. Pectus excavatum also develops in those with inborn errors of surfactant metabolism surviving beyond infancy, as illustrated on a CT image (**B**) of a 4-year-old with *ABCA3* gene mutations.

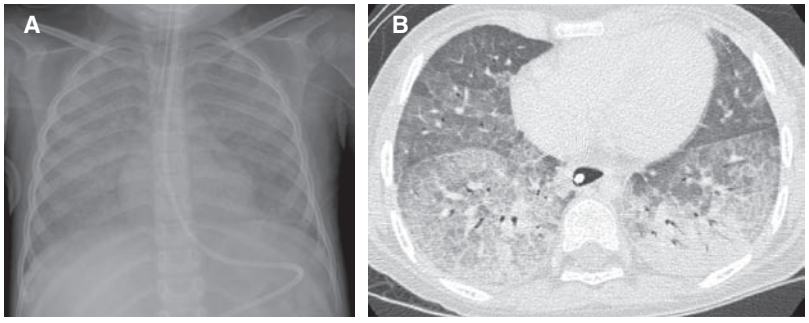

FIG. 35. Pulmonary alveolar proteinosis attributable to a GM-CSF-alpha-receptor defect in a 3-year-old manifests with diffuse airspace opacification on CXR (**A**) and consolidation, ground-glass opacification, septal thickening, and crazy-paving on HRCT (**B**).

obstruction, such as from hypoplastic left heart syndrome, total anomalous pulmonary venous return, pulmonary vein stenosis, pulmonary vein atresia, or cor triatriatum.

Pulmonary lymphangiectasia classically presents as severe respiratory distress in term neonates with diffuse hazy opacification of the lungs on CXR resembling the findings of surfactant deficiency of prematurity or inborn errors of surfactant metabolism. HRCT shows a characteristic constellation of smooth thickening of the septa and bronchovascular bundles, patchy perihilar and subpleural ground-glass opacities, pleural thickening, and effusions (often chylous). In those surviving the neonatal period, the lungs become clearer and interstitial thickening decreases but hyperinflation increases with age. Patchy ground-glass opacities that are fixed in location may be observed. Pectus excavatum develops in one-third of cases.[63–65]

In lymphangiomatosis, there is a proliferation of complex anastomosing lymphatic channels with secondary lymphatic dilation. Pulmonary lymphangiomatosis can be difficult to differentiate from pulmonary lymphangiectasia, since the histopathologic and radiographic findings in the lungs are very similar and chylous pleural effusions are common in both.[65,66] As distinguishing features, lymphangiomatosis most often presents in late childhood and frequently involves extrapulmonary tissues, with lytic bone lesions and mediastinal soft tissue edema commonly observed[67,68] (Fig. 36).

Pulmonary Veno-Occlusive Disease and Pulmonary Capillary Hemangiomatosis

The obstructive process of the pulmonary venules in PVOD and alveolar capillary bed in pulmonary capillary hemangiomatosis (PCH) results in pulmonary arterial hypertension, low or normal pulmonary vein pressure, and transudative pulmonary edema. These hemodynamic alterations produce the constellation of CT findings of smooth septal thickening, ground-glass opacities (diffuse, mosaic, or centrilobular), consolidation, pleural effusions, central pulmonary artery and right heart chamber enlargement, normal left atrial and ventricular contours, and normal-caliber main pulmonary veins (Fig. 37). PCH manifests with less pronounced septal thickening and better defined nodular ground-glass opacities than PVOD. The pulmonary imaging findings of PVOD and PCH have marked similarity with those seen in pulmonary vein stenosis, pulmonary vein atresia, total anomalous pulmonary venous return, cor triatriatum, left heart failure, and pulmonary lymphangiomatosis or lymphangiectasia, and attention to the pulmonary veins and cardiomediastinal structures can aid in distinction of these disorders. It is important not to misdiagnose PVOD or PCH as primary pulmonary hypertension or pulmonary thromboembolic disease, since the vasodilators used to treat primary pulmonary arterial hypertension can induce fulminant pulmonary edema in patients with PVOD or PCH. Primary pulmonary hypertension and pulmonary thromboembolic disease may exhibit pulmonary artery enlargement and mosaic lung attenuation, but septal thickening, centrilobular opacities, and pleural effusions are usually not a feature, facilitating distinction from PVOD and PCH.[69]

Diffuse Pulmonary Lymphoid Hyperplasia

Follicular bronchitis/bronchiolitis and LIP fall in the spectrum of "diffuse pulmonary lymphoid hyperplasia" that develops in response to viral infection (eg, EBV, HIV, HHV-6),

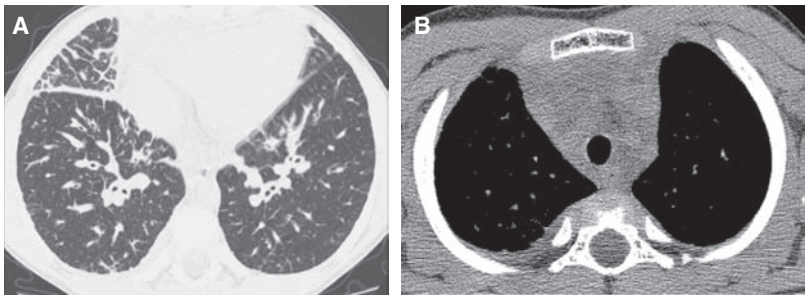

FIG. 36. Chest CT images of a 6-year-old viewed at lung windows (**A**) and soft tissue windows (**B**) shows thickening of the septae and bronchovascular bundles, as well as a small right pleural effusion and mediastinal edema characteristic of thoracic lymphangiomatosis.

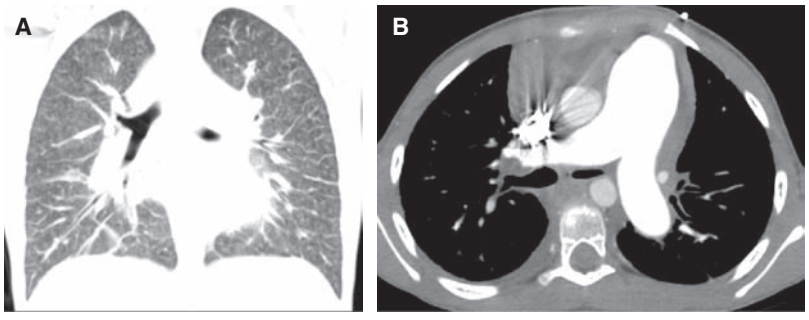

FIG. 37. In a 7-year-old with pulmonary hypertension and cor pulmonale, a coronal chest CT image viewed at lung windows (**A**) shows smooth septal thickening and ill-defined ground-glass centrilobular opacities, while an axial chest CT image viewed at soft tissue windows (**B**) demonstrates a right pleural effusion and marked pulmonary artery enlargement. This constellation of findings reflects the hemodynamic alterations in the pulmonary circulation resulting from pulmonary veno-occlusive disease (PVOD).

autoimmune disease (especially Sjogren's syndrome), immunodeficiency, or an unknown trigger.[70] Follicular bronchitis/bronchiolitis is characterized by prominent peribronchial lymphoid follicles while LIP is characterized by an interstitial lymphocytic infiltrate.

Follicular bronchitis/bronchiolitis typically presents by 6–8 weeks of age with unremitting respiratory distress and fever. At the initial presentation, CXR shows hyperinflation and peribronchial thickening resembling the findings of acute lower airway infection or reactive airways disease.[71] Evolution to LIP occurs over several months as the radiographic findings sequence from peribronchial thickening to fine reticular opacities, reticulonodular opacities, and coalescent nodules forming confluent opacities. HRCT reveals micronodules of 1–3 mm diameter in a perilymphatic interstitial distribution (subpleural > septal> centrilobular> peribronchovascular) with a basilar predominance[72,73] (Fig. 38). Bronchiectasis develops in 3% of cases at a follow-up period of 3–7 years,[74] and formation of cysts has also been described.[75] With the exception of bronchiectasis, the pulmonary findings potentially reverse in response to antiretroviral therapy or in the natural course of the disease.[74]

LIP occurs in 30%–40% of children infected with human immunodeficiency virus (HIV). In 1987, the CDC formulated criteria for a presumptive diagnosis of LIP to differentiate it from mycobacterial, viral, and fungal infections, and obviate the need for lung biopsy. These criteria include diffuse, symmetric, reticulonodular, or nodular pulmonary opacities that persist for at least 2 months with no identifiable pathogen or response to antibiotic therapy. A recent systematic literature review of the radiologic features of LIP in HIV-infected children found that 75%–92% of all biopsy-proven cases of LIP in HIV-infected children would be diagnosed using the 1987 CDC criteria for a presumptive diagnosis, supporting the continued validity of the criteria. In 20% of cases of LIP in the review, mediastinal abnormalities attributable to lymphadenopathy were recorded, although miliary tuberculosis should still be considered if lymphadenopathy is present.[74]

Bronchiolitis Obliterans

The most common abnormality on CXR in patients with bronchiolitis obliterans is hyperinflation, but the findings are often nonspecific and the CXR can be normal.[76] Both lung ventilation-perfusion scintigraphy and CXR are less sensitive than HRCT for bronchiolitis obliterans.[77] The characteristics findings of bronchiolitis obliterans on HRCT are mosaic attenuation, air trapping, pulmonary vascular attenuation, bronchial wall thickening, and bronchiectasis (Fig. 39). Bronchiolitis obliterans can be confidently diagnosed in children on the basis of clinical presentation (especially a history of viral or *Mycoplasma* infection, graft-versus-host disease, Stevens–Johnson syndrome, or lung transplantation), fixed obstructive lung disease on pulmonary function testing, and characteristic findings on HRCT, obviating the need for lung biopsy.[76] In fact, the heterogeneous distribution of airway involvement by bronchiolitis obliterans can lead to sampling error, and lung biopsies are normal or nondiagnostic in up to one-third of children with bronchiolitis obliterans.[78]

Swyer-James-MacLeod syndrome is a particular form of bronchiolitis obliterans characterized on CXR by a small- or normal-sized hyperlucent lung with decreased vascularity presenting several months or a few years after the precipitating infection. Although the abnormalities may appear to be unilateral on CXR, HRCT reveals that the findings of

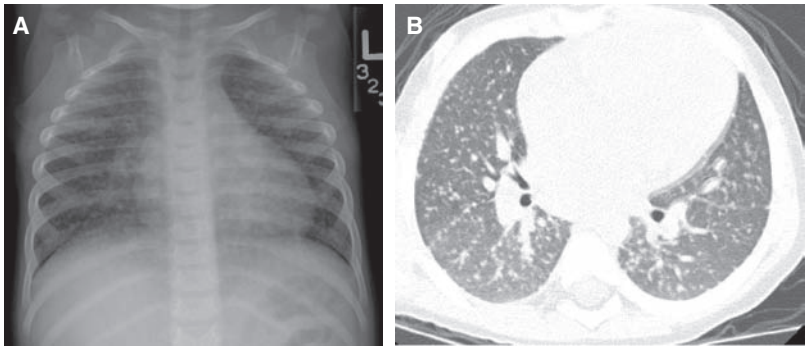

FIG. 38. CXR (**A**) and chest CT (**B**) images show numerous tiny pulmonary nodules in a perilymphatic interstitial distribution in a child with lymphoid interstitial pneumonia.

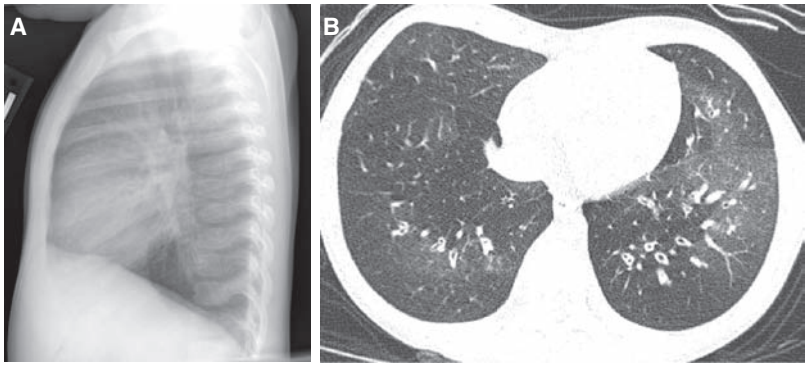

FIG. 39. The lateral CXR (**A**) of a 2-year-old with recurrent wheezing following adenovirus pneumonia shows diaphragmatic flattening consistent with pulmonary hyperinflation. An image from an HRCT exam (**B**) obtained at 4 years of age reveals characteristics findings of bronchiolitis obliterans, including mosaic attenuation, pulmonary vascular attenuation in hyperlucent areas, bronchial wall thickening, and bronchiectasis.

bronchiolitis obliterans, including mosaic attenuation and air trapping, are bilateral in about one-half of cases of Swyer-James-MacLeod syndrome[79] (Fig. 40).

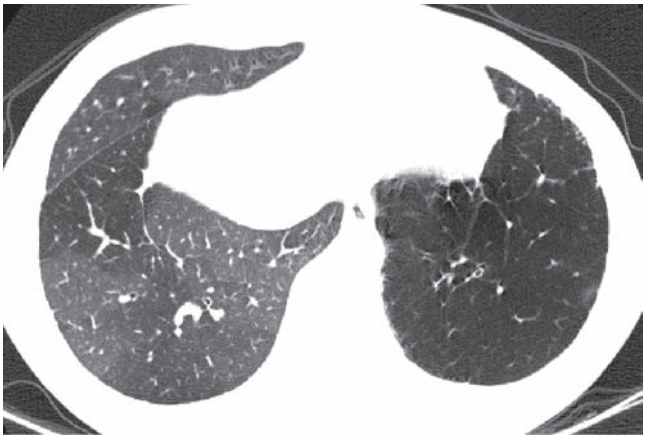

FIG. 40. A chest CT image from a teenager with Swyer-James-MacLeod syndrome shows a small hyperlucent left lung with attenuated pulmonary vasculature. Mosaic attenuation related to bronchiolitis obliterans is also observed in the right lung.

Hypersensitivity Pneumonitis

Hypersensitivity pneumonitis, also known as extrinsic allergic alveolitis, is usually precipitated in children by exposure to organic antigens from birds or fungi. The diagnosis of hypersensitivity pneumonitis is supported by a history of exposure, the presence of precipitating antibodies, and the observation of compatible imaging findings.[80] In acute hypersensitivity pneumonitis, the CXR may show opacities resembling pulmonary edema or pneumonia within the mid and lower lung zones. However, a normal CXR does not exclude hypersensitivity pneumonitis, and 40% of the cases with a normal CXR have pulmonary abnormalities visible by HRCT. As with CXR, the acute phase on HRCT is characterized by opacities that may mimic infection or edema. In the subacute phase, HRCT reveals poorly defined centrilobular nodules, ground-glass opacities, and air trapping. There is relative sparing of the upper lung zones in the acute and subacute phases. Subpleural irregular linear opacities, architectural distortion, and honeycombing related to pulmonary fibrosis are found on HRCT in the chronic phase. HRCT often shows findings associated with multiple phases concurrently related to ongoing antigen exposure prior to diagnosis (Fig. 41). The clinical symptoms typically resolve within a few days of starting treatment and ceasing exposure to the inciting antigen, although it may take several weeks for the HRCT findings of acute and subacute hypersensitivity pneumonitis to resolve. The findings of pulmonary fibrosis on HRCT persist and may even progress despite elimination of exposure to the offending antigen.[29,81]

Diffuse Pulmonary Hemorrhage Disorders

Diffuse pulmonary hemorrhage disorders can be classified by etiology and grouped according to the presence or absence of pulmonary capillaritis, a pathologic process characterized by inflammatory disruption of the capillary network of the interstitium. Pulmonary hemorrhage disorders with capillaritis include idiopathic pulmonary capillaritis, Wegener's granulomatosis, microscopic polyangiitis, Goodpasture's syndrome, idiopathic pulmonary-renal syndrome, lupus, and drug-induced capillaritis. Pulmonary hemorrhage disorders without capillaritis include IPH, acute idiopathic pulmonary hemorrhage of infancy, Heiner syndrome, coagulation disorders, and cardiovascular disorders (eg, PVOD, pulmonary arteriovenous malformations).[82]

Hemoptysis is present in only a minority of children with diffuse pulmonary hemorrhage, but most have anemia and an abnormal CXR on presentation.[83] The classic CXR appearance of acute diffuse pulmonary hemorrhage is described as a "butterfly" or "batwing" pattern of symmetric airspace opacities. However, the opacities may be asymmetric or unilateral.[83,84] HRCT is more sensitive than CXR for pulmonary hemorrhage and shows patchy ground-glass opacities and consolidation in the acute phase, reflecting filling of the airspaces with blood.[83,84] Hemosiderin-laden macrophages aggregate in the interstitium after repetitive or chronic hemorrhage, resulting in septal thickening and nodular opacities. Crazy-paving may also be observed[58,85,86] (Fig. 42).

The imaging findings of pulmonary hemorrhage are not specific, although certain features favor particular disorders.[82] Capillaritis should be suspected if small fluffy or centrilobular perivascular opacities are present (Fig. 43). These opacities reflect the angiocentric inflammation and hemorrhage associated with capillaritis, and biopsy may be obviated in the appropriate clinical setting.[87] IPH usually presents before the age of 3 years and is linked with certain household molds and decreased levels of von Willebrand factor, suggesting an environmental trigger in genetically predisposed individuals. IPH is occasionally associated with lymphadenopathy and celiac disease, suggesting an autoimmune etiology in these cases.[53,57,58,86]

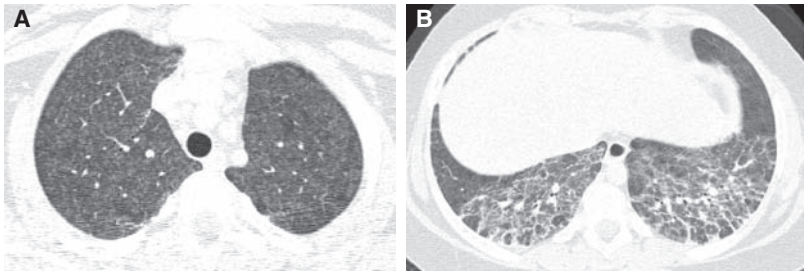

FIG. 41. HRCT images of a 10-year-old with cough, fatigue, and hypoxemia following exposure to chickens demonstrate diffuse ill-defined ground-glass centrilobular nodular opacities involving the upper lung zones (**A**) and irregular linear opacities at the posterior lung bases (**B**). These findings are consistent with concurrent subacute and chronic phases of hypersensitivity pneumonitis from ongoing antigen exposure prior to diagnosis.

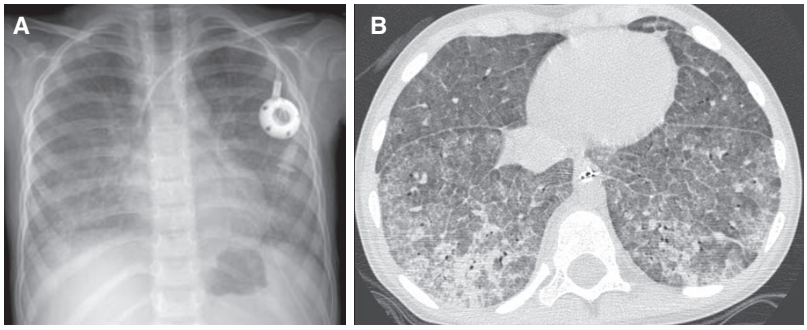

FIG. 42. A 4-year-old with anemia and hemoptysis exhibits symmetric perihilar and medial basilar pulmonary airspace opacities on CXR (**A**) and patchy consolidation, ground-glass opacities, septal thickening, and crazy-paving on HRCT (**B**), reflecting the effects of combined acute and chronic pulmonary hemorrhage.

Pulmonary Alveolar Microlithiasis

Pulmonary alveolar microlithiasis is an autosomal recessive disease associated with mutations of the solute carrier family 34 subfamily A isoform 2 (*SLC34A2*) gene that encodes a sodium-dependent phosphate transporter expressed in alveolar type II cells. Inability of alveolar type II cells to clear phosphorus ions likely leads to the characteristic accumulation of calcium phosphate microliths in the alveoli, subpleural space, interlobular septa, and bronchovascular bundles. The pathologic and radiologic findings correlate well, with CXR showing sand-like micronodules scattered throughout the lungs and obliterating the mediastinal and diaphragmatic contours in advanced cases (Fig. 44). HRCT demonstrates calcified micronodules (<3 mm diameter) with thickening of interlobular septa, bronchovascular bundles, and fissures. Ground-glass opacities, consolidation, and small cysts are also commonly observed in pulmonary alveolar microlithiasis on HRCT. Involvement is most pronounced of the posterior lower lobes and anterior upper lobes, and the calcifications are rendered more conspicuous by using soft tissue window settings rather than lung window settings. The differential diagnosis of calcified micronodules includes miliary tuberculosis, pulmonary hemosiderosis, and metastatic calcinosis associated with chronic renal failure, and distinction is usually possible by appropriate clinical correlation.[88]

The degree of pulmonary function loss correlates with the extent of pulmonary parenchymal abnormalities on imaging in patients with pulmonary alveolar microlithiasis. Clinical symptoms are usually absent or very mild in earlier stages of pulmonary alveolar microlithiasis, and the diagnosis of clinically occult cases can often be established by CXR or CT screening of the relatives of the index patient.[89]

Nonspecific Interstitial Pneumonia

Nonspecific interstitial pneumonia (NSIP) bears an unfortunate name because it is associated with a distinct histologic appearance. It is characterized on pathology by spatially and temporally uniform interstitial inflammation with varying degrees of fibrosis. In children, it can be idiopathic, familial, or affiliated with certain conditions, including

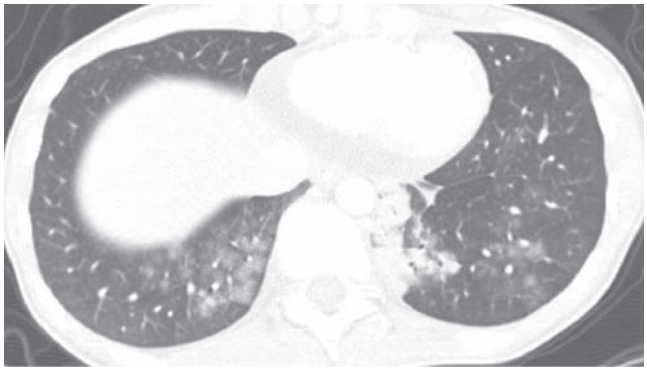

FIG. 43. A chest CT image from a 15-year-old with pulmonary capillaritis demonstrates multiple fluffy nodular opacities at the lung bases resulting from angiocentric inflammation and hemorrhage.

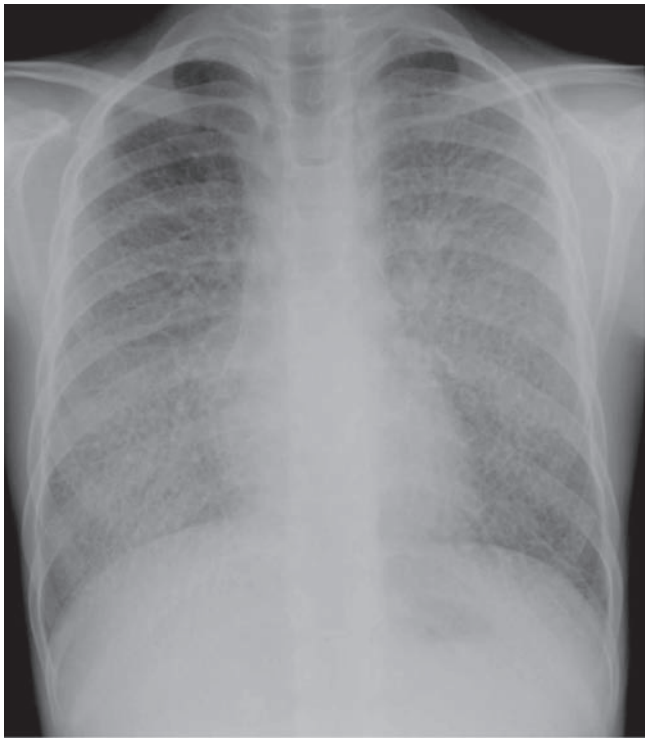

FIG. 44. A CXR of a 12-year-old with pulmonary alveolar microlithiasis shows numerous pulmonary micronodules with relative sparing of the apices (image courtesy of Robin Deterding, M.D.).

FIG. 45. An HRCT image from an 11-year-old with familial NSIP shows fine linear and ground-glass opacities at the lung periphery and a few subtle subpleural cysts.

but the fibrosis may be advanced before clinical symptoms manifest. There is no clear correlation between the duration of illness and the severity of lung involvement, but the severity of lung involvement on HRCT correlates with deficits in pulmonary function testing. Early detection of lung involvement by HRCT surveillance may be beneficial by directing prompt treatment to prevent irreversible pulmonary fibrosis.[91,92]

Findings of lung involvement are noted on CT in 25% of patients with juvenile-onset mixed connective tissue disease. These findings include a microcystic reticular pattern with fine intralobular and ground-glass opacities, evocative of NSIP. The lung involvement is predominantly mild with a median disease extent of 2% of the lung parenchyma.[93]

Studies reporting thoracic involvement by systemic lupus erythematosus (SLE) consist largely of adult patients and

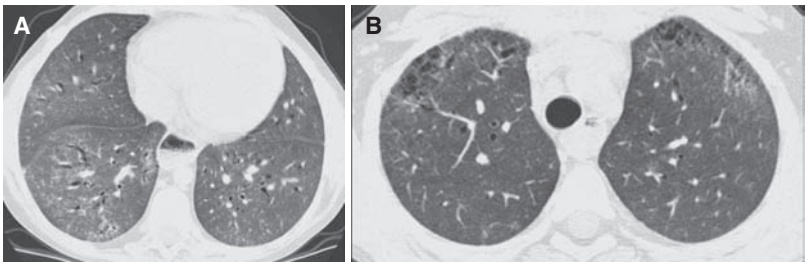

FIG. 46. HRCT images of NSIP in a 10-year-old with systemic sclerosis show fine linear and ground-glass opacities (**A**) and coalescent subpleural cysts resembling honeycombing (**B**). Esophageal dilation related to the systemic sclerosis is also demonstrated.

autoimmune connective tissue disorders and inborn errors of surfactant metabolism.[5,53]

The HRCT findings most often seen with NSIP are ground-glass and fine linear or reticular opacities predominantly at the lung periphery (Fig. 45). Consolidation and cysts are occasionally seen. Traction bronchiectasis, volume loss, and honeycombing may develop over time. The HRCT findings of NSIP can resolve or persist, depending on the degree of fibrosis.[90]

Connective Tissue and Collagen-Vascular Diseases

The use of HRCT has revealed a high prevalence of interstitial lung disease, particularly NSIP, in those with connective tissue and collagen-vascular diseases such as systemic sclerosis and dermatomyositis. The pulmonary findings on HRCT scans have limited specificity for distinguishing among these diseases, although ancillary findings may provide a clue to the specific diagnosis, such as the presence of esophageal dilation that suggests systemic sclerosis.[27,90]

Lung involvement is an adverse prognostic factor in juvenile systemic sclerosis, and evidence of lung involvement in present on HRCT in 53% of children with systemic sclerosis at initial assessment.[91] The HRCT findings of lung involvement in systemic sclerosis often present in an NSIP pattern, with fine reticular or ground-glass opacities principally involving the lung periphery.[27] Subpleural micronodules, subpleural cysts, traction bronchiectasis, and honeycombing may also be observed (Fig. 46). Only a subset of patients develops progressive pulmonary fibrosis, describe the most common CT findings as interlobular septal thickening, parenchymal bands, bronchiectasis, mediastinal lymphadenopathy, and pleuropericardial effusions.[94] In distinction to adult-onset SLE, interstitial lung disease is uncommon in childhood-onset SLE, with only 8% of patients having abnormal findings on HRCT. This suggests that asymptomatic children with SLE do not need HRCT screening.[95] When the lungs are involved in childhood-onset SLE, it is frequently in the form of vasculitis with pulmonary hemorrhage (Fig. 47).

FIG. 47. Ground-glass opacities centered around the pulmonary vasculature on this HRCT image of a 14-year-old with systemic lupus erythematosus represent foci of hemorrhage from pulmonary vasculitis.

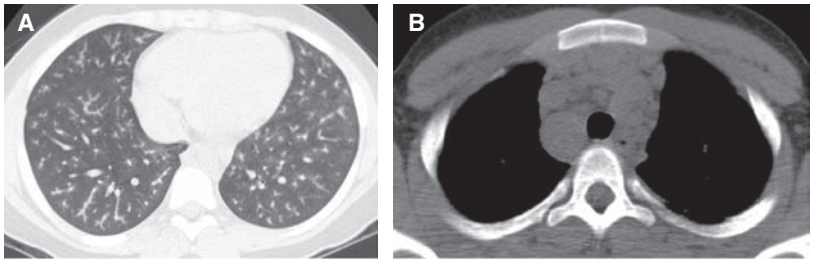

FIG. 48. In a 12-year-old with pulmonary sarcoidosis, the presence of perilymphatic nodules gives a beaded appearance to the bronchovascular bundles on a chest CT image viewed at lung windows (**A**). Mediastinal lymphadenopathy is revealed on a chest CT image viewed at soft tissue windows (**B**).

Lung involvement is reported to occur in 55%–92% of pediatric patients with sarcoidosis and is more common in children older than 8 years of age than in younger children. The majority (89%–100%) of these children present with hilar lymphadenopathy, which is bilateral in most cases. Isolated lung involvement without lymphadenopathy is uncommon, being found in only 11% of cases, and is usually interstitial rather than alveolar.[96] The typical HRCT findings of sarcoidosis are peribronchovascular and interstitial thickening, and small well-defined pulmonary nodules that may be interlobular, centrilobular, or peribronchovascular in distribution. The nodules give a beaded appearance to the bronchovascular bundles and interlobular septa[97] (Fig. 48).

Organizing Pneumonia

Organizing pneumonia in children can be idiopathic or secondary to infection, asthma, drug reaction, aspiration pneumonia, autoimmune disease, chemotherapy, bone marrow transplantation, or other disorders that incite a reparative response in the lung.[98] Organizing pneumonia is characterized histologically by intraluminal organizing fibrosis in the distal airways and airspaces (bronchioles, alveolar ducts, and alveoli). The appearance of organizing pneumonia on CT is variable, with the most frequent pattern consisting of peripheral patchy consolidations with or without surrounding ground-glass-like opacities. Air bronchograms and mild bronchial dilation are common within the consolidations (Fig. 49). Other patterns include central ground-glass opacity surrounded by consolidation (atoll or reverse halo sign), small pulmonary nodules along bronchovascular bundles, linear and band-like subpleural opacities, perilobular thickening, and progressive fibrosis.[99] Differential diagnostic considerations include infectious pneumonia, vasculitis, and eosinophilic pneumonia.[1]

Acute Interstitial Pneumonia and Diffuse Alveolar Damage

Diffuse alveolar damage (DAD) is a histopathologic pattern characterized by an exudative phase exhibiting edema, hyaline membranes, and interstitial acute inflammation, and an organizing phase exhibiting loose organizing fibrosis, mostly within the alveolar septa, and Type II pneumocyte hyperplasia. DAD is associated with acute respiratory distress syndrome (ARDS), infection (especially CMV or *Pneumocystis*), bone marrow transplantation, and primary graft dysfunction in lung transplant recipients. DAD is also associated with the clinicopathologic diagnosis of idiopathic AIP in previously healthy children, and has a poor prognosis. The initial HRCT findings of AIP/DAD are patchy or geographic ground-glass opacity, consolidation, and sometimes crazy-paving, followed by architectural distortion and traction bronchiectasis (Fig. 50). The differential diagnosis includes infectious pneumonitis, hydrostatic pulmonary edema, PAP, pulmonary hemorrhage, and acute eosinophilic pneumonia (AEP).[3,98]

Lipoid Pneumonia

Endogenous lipoid pneumonia arises from PAP or an obstructed airway leading to the accumulation of cholesterol and other lipids in the distal airspaces, while exogenous lipid pneumonia arises from aspiration of mineral, vegetable, or animal oils. Exogenous lipoid pneumonia in the pediatric population is most frequently associated with mineral oil use for chronic constipation. Neonates and children with swallowing dysfunction related to neurologic or neuromuscular disorders are at higher risk of exogenous lipoid pneumonia, although oropharyngeal dysphagia and silent aspiration can occur even in developmentally appropriate infants and young children. Those with exogenous lipoid pneumonia may be asymptomatic or have nonspecific symptoms such as cough, tachypnea, or fever, and the relevant clinical history may not be proffered. Consequently, lipoid pneumonia may be unsuspected, and the diagnosis may be first suggested on the basis of the radiographic findings.

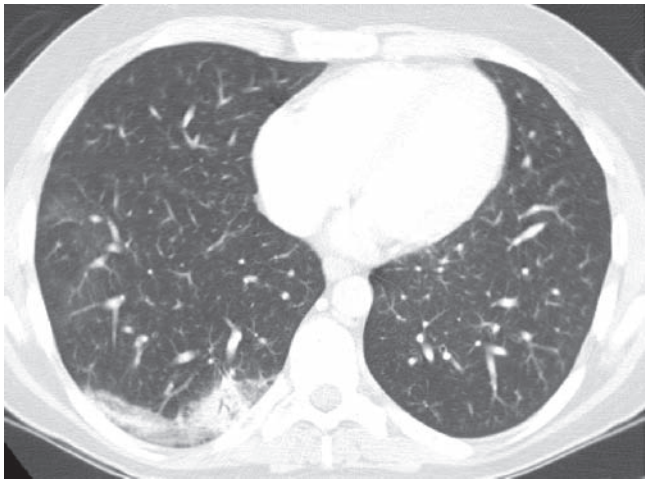

FIG. 49. A chest CT image of an 18-year-old with graft-versus-host-disease shows patchy ground-glass opacity and consolidation with air bronchograms at the periphery of the right lower lobe, consistent with organizing pneumonia.

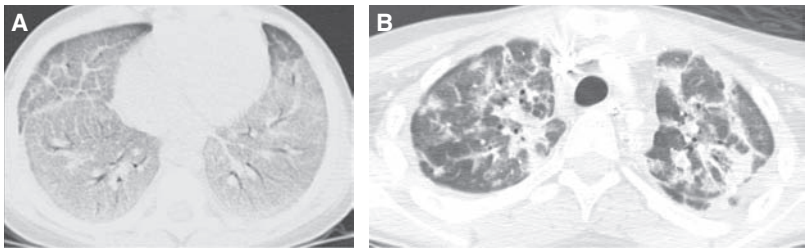

FIG. 50. Diffuse alveolar damage is the histopathologic correlate in this infant with respiratory failure and crazy-paving on chest CT (**A**) and in this teenage lung transplant recipient with primary graft dysfunction and patchy ground-glass opacity and consolidation on chest CT (**B**).

FIG. 51. An HRCT image from a 17-year-old with a history of mineral oil use for chronic constipation depicts a crazy-paving pattern attributable to exogenous lipoid pneumonia.

The most common CT finding in exogenous lipoid pneumonia is consolidation, predominantly in the central and posterior aspects of the lower lobes and right upper lobe. Ground-glass opacities, nodules, and a crazy-paving pattern may also be observed (Fig. 51). The consolidation usually contains characteristic foci of fatty attenuation, but in some cases the fat attenuation is not evident because of volume averaging with adjacent inflammatory exudates. Also, volume averaging of air and inflammatory exudates in other forms of pneumonitis can produce foci of seeming fat attenuation and result in a false positive impression of lipoid pneumonia.[100,101]

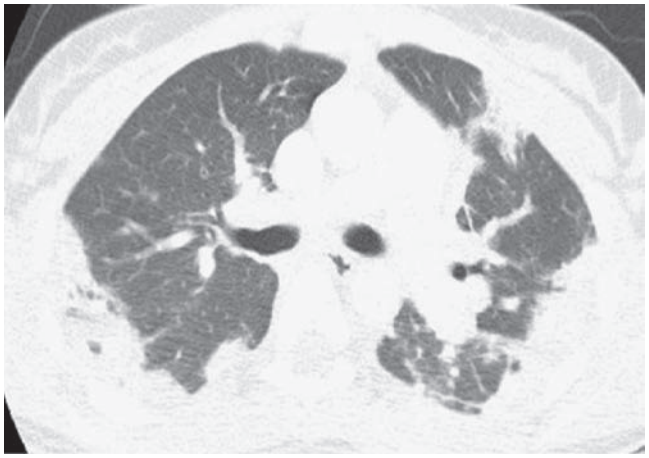

FIG. 52. A chest CT image from an 18-year-old with dyspnea and peripheral eosinophilia induced by minocycline demonstrates peripheral consolidations sparing the central lung zones, characteristic of drug-induced eosinophilic pneumonia.

Pulmonary Infiltrate With Eosinophilia

Disorders under the rubric of pulmonary infiltrate with eosinophilia (PIE) include simple pulmonary eosinophilia (SPE, or Löffler's syndrome), chronic eosinophilic pneumonia (CEP), AEP, idiopathic hypereosinophilic syndrome (IHS), allergic bronchopulmonary aspergillosis (ABPA), bronchocentric granulomatosis (BG), allergic angiitis and granulomatosis (Churg–Strauss syndrome), drug-induced PIE, and PIE induced by parasitic infection. Peripheral eosinophilia is usually present in these disorders, but can be absent in AEP.

The associated radiographic findings of interstitial, alveolar, or mixed interstitial/alveolar pulmonary opacities are often nonspecific, although a specific diagnosis can be suggested in some instances. The pattern of peripheral consolidations sparing the central lung zones ("photographic negative of pulmonary edema") coupled with peripheral eosinophilia allows a presumptive diagnosis of CEP or drug-induced PIE (Fig. 52). ABPA presents with central bronchiectasis with or without mucoid impaction. Pulmonary nodules with ground-glass halos are characteristic of SPE and IHS. AEP without peripheral eosinophilia can simulate ARDS, AIP, or hydrostatic pulmonary edema with airspace opacities, septal thickening, and pleural effusions. BG manifests with focal masses and nodules or lobar consolidation with atelectasis. Findings in Churg–Strauss syndrome include subpleural consolidation, centrilobular nodules, bronchial wall thickening, and interlobular septal thickening. Even if the findings are nonspecific, imaging localizes potential sites for lung biopsy and provides a noninvasive method to evaluate response to therapy.[102,103]

Langerhans Cell Histiocytosis

Langerhans cell histiocytosis (LCH) is characterized by granulomatous infiltration of various tissues by large dendritic cells (Langerhans cells). In later stages, the granulomas may be replaced by fibrosis, scarring, and cyst formation. Childhood pulmonary LCH is clonal and is unassociated with smoking, distinguishing it from adult pulmonary LCH. With rare exception, pulmonary LCH in children is observed only in the setting of multisystem LCH. Pulmonary involvement is present in a minority of cases of multisystem LCH, and most cases initially present with a skin rash in infancy.[104,105]

Diffuse reticulonodular opacities constitute the most common appearance of childhood pulmonary LCH on CXR. Cysts, often irregular in shape, are seen in 31% of cases. Spontaneous pneumothorax can complicate cyst rupture. Thymic involvement is common, especially in multisystem disease, and serves as a potential clue to the diagnosis. Thymic involvement is suggested by the presence of thymic enlargement, particularly if intrathymic calcifications, cysts, or cavitations are present[106] (Fig. 53).

Only one-half of the patients with lung involvement on imaging present with respiratory symptoms or signs, and lung imaging should be performed in all newly diagnosed LCH patients. Lung involvement usually parallels overall disease activity, but the severity of lung involvement is not predictive of outcome in children despite the designation of the lung as a risk organ in the treatment protocols of the Histiocyte Society. Of children treated for LCH, 6% have asymptomatic lung involvement at a mean of 15 years off-treatment.[104,105]

Storage Diseases

Gaucher disease and Niemann–Pick disease are lysosomal storage disorders in which lipid-laden "foamy" macrophages (Gaucher cells or Niemann–Pick cells) accumulate in various tissues. The lipid-laden macrophages occupy the alveoli, thicken the alveolar walls, and fill the peribronchovascular, subpleural, and interlobular lymphatic spaces. Pulmonary abnormalities in children with lysosomal storage disorders can be also be caused by repeated pneumonia from immunologic deficits or chronic aspiration from neurologic deficits.

Symptomatic lung involvement by Gaucher disease is rare at presentation, but develops later in the disease course in some patients, especially those with neuronopathic type III. Respiratory failure from interstitial lung disease is second only to hepatic failure as a cause of death in young patients with type III Gaucher disease. CXR may demonstrate reticulonodular opacities in Gaucher disease, while HRCT displays a broader range of abnormalities including ground-glass opacities, consolidation, interstitial thickening, and bronchial wall thickening. Hilar and mediastinal lymphadenopathy are common, and thymic enlargement may also be noted in Gaucher disease.[107] In children with Gaucher disease receiving enzyme replacement therapy, gradual improvement of the pulmonary abnormalities can be noted radiographically, although complete reversal does not occur and significant pulmonary involvement may persist.[108]

In Niemann–Pick disease, lung involvement is most common in the type B form in which a nonspecific reticulonodular interstitial pattern is usually observed. The progression of lung disease in Niemann–Pick type B is slow and respiratory symptoms are usually mild, and chest imaging has not proven useful for determining the severity or outcome of lung involvement.[109] In distinction, lung disease in Niemann–Pick type 2C is characterized by respiratory distress presenting in infancy from PAP due to alveolar overfilling with dysfunctional cholesterol-laden surfactant[54] (Fig. 54).

Diagnostic Efficacy of Imaging ChILD

In one study of diffuse pediatric lung disease, diagnoses were made with a high degree of confidence in 62% of HRCT interpretations, compared with only 12% of CXR interpretations. By HRCT, 56% of the confident first-choice diagnoses were correct, compared with 40% for CXR, and 40% of all HRCT first-choice diagnoses were correct, compared with 28% for CXR. The correct diagnosis was included as 1 of the 3 top diagnostic choices in 58% of the HRCT interpretations, compared with 48% for CXR. Diagnoses were most accurate for bronchiolitis obliterans, organizing pneumonia, hypersensitivity pneumonitis, and lymphangiomatosis, and least accurate for disorders with consolidation or ground-glass opacities. The accuracy of HRCT for diffuse lung disease in children is less than it is for adults.[110] In another study of diffuse pediatric lung disease, a correct first-choice diagnosis was made in 61% of the cases on HRCT compared with 34% on CXR. The correct diagnosis was listed among the diagnostic considerations in 66% of HRCT cases versus 45% of CXR cases. Confident diagnoses were more likely to be correct with HRCT (91%) than with CXR (70%). Findings were more confidently classified as normal on HRCT than on CXR. PAP and pulmonary lymphangiectasia were correctly diagnosed on HRCT with a high degree of confidence.[66] In a more recent study of diffuse pediatric lung disease, a correct first-choice diagnosis was made by HRCT in only 38% of cases and the correct diagnosis was among the 3 main choices in 59% of cases. PAP was the disease most frequently diagnosed correctly. Lymphangiectasia and LCH were also correctly diagnosed, while hypersensitivity pneumonitis, connective tissue disease, sarcoidosis, and IPH were rarely recognized.[57]

The likelihood of making a correct diagnosis by imaging depends not only on the type of diffuse lung disease, but also on the quality of the imaging study and the expertise of the interpreter. It is important to recognize the limitations

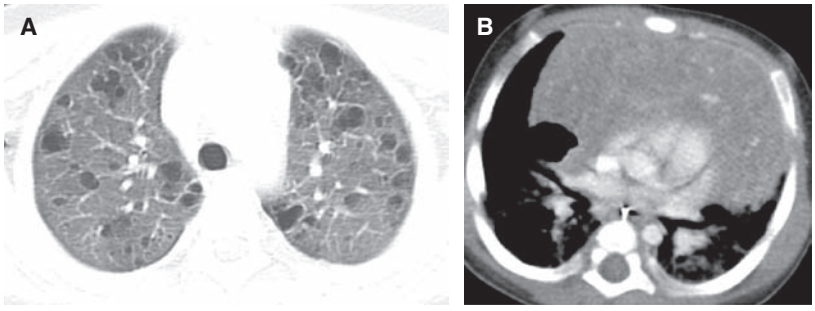

FIG. 53. An HRCT image viewed at lung windows (**A**) shows numerous thin-walled cysts of various shapes in an 8-year-old with pulmonary Langerhans cell histiocytosis. A contrast-enhanced chest CT image viewed at soft tissue windows (**B**) shows a cavitation and calcifications within an enlarged thymus in an infant with multisystem Langerhans cell histiocytosis.

FIG. 54. In an infant with Niemann–Pick type 2C disease, overfilling of the airspaces by cholesterol-laden surfactant causes pulmonary alveolar lipoproteinosis and a crazy-paving pattern on an HRCT image.

of imaging and radiologists. Even specialists in pediatric thoracic radiology, who are unavailable at many institutions, may achieve a correct first-choice diagnosis in <50% of cases.[111] The few published studies of diagnostic imaging performance are confounded by inconsistent results and the use of imprecise or outdated histopathologic classification schemes. Ongoing recognition of new disorders and reclassification of established disorders are problematic for comparing results of older studies, and correlative radiologic–pathologic studies based on the latest chILD Research Cooperative histopathologic classification scheme are gradually emerging.

For cost-effective, evidence-based clinical practice, it is imperative not only to evaluate diagnostic imaging performance but also to assess the marginal value of imaging relative to the history, physical exam, and laboratory data and the influence of imaging on patient management and outcome. One study found that the positive yield of CT for evaluation of pediatric acquired diffuse lung disease is only 23%, when the positive yield is defined as providing a diagnosis, excluding lung disease, identifying a previously unrecognized clinically important finding, or altering the plan for further evaluation or treatment.[111] The benefit of CT in chILD is underestimated by this study, since the use of CT for planning biopsy, providing prognostic information or determining response to therapy is overlooked. Still, CT must be used judiciously and appropriateness criteria need to be developed, especially in consideration of potential radiation risks to children from CT.

The optimal use of diagnostic imaging is aided by close collaboration between the clinician, radiologist, and pathologist. Diagnostic imaging often provides the first definitive evidence that a diffuse lung disease is present. A confirmatory lung biopsy may not be necessary if the radiologist is able to suggest a specific diagnosis, such as NEHI or bronchiolitis obliterans, in the appropriate clinical setting.[24,78] Even if the imaging findings are not specific for a certain diagnosis, the radiologist may be able to suggest a short list of the most likely diagnoses and thereby guide further investigation and potentially avert the need for lung biopsy.[5] For example, CT findings evocative of hypersensitivity pneumonitis, lipoid pneumonia, pulmonary hemorrhage, or an inborn error of surfactant metabolism can direct the next appropriate serologic assay, bronchoalveolar lavage, or genetic test.[66]

It is important to be mindful of extrapulmonary imaging findings that can assist in making a diagnosis, such as the presence of mediastinal edema in lymphangiomatosis, thymic enlargement and calcification in LCH, esophageal dilation in systemic sclerosis, and pectus excavatum in chronic surfactant dysfunction related to *ABCA3* gene mutations. It is also important to recognize that chILD is rare and the imaging findings of more common disorders such as congenital heart disease and infection can mimic chILD, particularly in the neonatal period. Clues to chILD in this setting include severe lung disease unresponsive to conventional management in a term infant, a family history of lung disease in infancy, and extrapulmonary malformations or anomalies.[112]

If the clinical presentation and imaging findings are indeterminate for a diagnosis and a lung biopsy is needed, CT can provide guidance for the lung biopsy.[5] Interstitial lung disease can be patchy and heterogeneous, raising the risk of sampling error. CT guidance allows specimens of more affected lung as well as more normal-appearing lung to be acquired, thus avoiding sampling of normal lung or advanced but nonspecific fibrosis.[113]

The findings on imaging can provide prognostic information by suggesting a diagnosis and identifying adverse risk factors.[29] NEHI has a favorable prognosis, while inborn errors of surfactant metabolism, diffuse developmental disorders, and lung growth disorders have a high mortality with no curative treatment other than lung transplantation in some cases. The presence of pulmonary hypertension is inferred by imaging findings of right ventricular hypertrophy and pulmonary artery enlargement, and is associated with higher mortality in infant chILD.[2] Honeycombing on imaging is indicative of irreversible pulmonary fibrosis.[29] Severe abnormalities on chest CT in children under 3 years of age with postinfectious bronchiolitis obliterans anticipate poor lung function several years later.[114]

HRCT is widely regarded as an essential tool for the initial evaluation of suspected chILD, but significant variation exists in the use of HRCT to screen asymptomatic patients for subclinical disease and to monitor disease status. Resolution of pulmonary abnormalities on HRCT may lag the clinical response in hypersensitivity pneumonitis[29] and PIE.[100] Findings on HRCT do not always correlate with pulmonary function testing and do not necessarily predict response to treatment or outcome. HRCT in connective tissue disease patients with normal pulmonary function tests and without pulmonary symptoms often reveals interstitial lung disease, but HRCT cannot predict which subset will progress to clinically significant pulmonary fibrosis.[91,115] The severity of lung involvement shown by HRCT is not predictive of outcome in children with LCH, and it is not unusual for asymptomatic lung abnormalities to persist on HRCT for many years after treatment.[104,105] Changes in CT findings over time do not correlate with lung function or outcome in children with surfactant dysfunction related to *ABCA3* gene mutations.[52] In the absence of clear guidelines, clinical

judgment must direct the selection and timing of imaging in the management of chILD.[12]

Conclusion

Careful attention to technique is necessary to obtain high-quality chest imaging studies of children with suspected diffuse lung disease. Proper interpretation of these studies requires familiarity with the imaging features of the various forms of chILD, some of which exhibit a characteristic pattern that allows a specific diagnosis to be made, while others manifest with a nonspecific appearance requiring further investigation for a definitive diagnosis. HRCT continues to be the preferred imaging study for the initial evaluation of suspected chILD, but the role of HRCT in the screening of asymptomatic patients and in the monitoring of disease status is not well established. Ongoing technical advances in medical imaging promise better image quality, lower radiation risk, and improved guidance for the diagnosis and management of children with interstitial lung disease.

Author Disclosure Statement

No competing financial interests exist.

References

1. American Thoracic Society; European Respiratory Society. American Thoracic Society/European Respiratory Society International Multidisciplinary Consensus Classification of the Idiopathic Interstitial Pneumonias. This joint statement of the American Thoracic Society (ATS), and the European Respiratory Society (ERS) was adopted by the ATS board of directors, June 2001 and by the ERS Executive Committee, June 2001. Am J Respir Crit Care Med 2002;165:277–304.
2. Deutsch GH, Young LR, Deterding RR, Fan LL, Dell SD, Bean JA, Brody AS, Nogee LM, Trapnell BC, Langston C, Albright EA, Askin FB, Baker P, Chou PM, Cool CM, Coventry SC, Cutz E, Davis MM, Dishop MK, Galambos C, Patterson K, Travis WD, Wert SE, White FV; Pathology Cooperative Group; ChILD Research Co-operative. Diffuse lung disease in young children: application of a novel classification scheme. Am J Respir Crit Care Med 2007; 176:1120–1128.
3. Clement A; ERS Task Force. Task force on chronic interstitial lung disease in immunocompetent children. Eur Respir J 2004; 24:686–697.
4. Lynch DA, Brasch RC, Hardy KA, Webb WR. Pediatric pulmonary disease: assessment with high-resolution ultrafast CT. Radiology 1990; 176:243–248.
5. Brody AS. Imaging considerations: interstitial lung disease in children. Radiol Clin North Am 2005; 43:391–403.
6. Mayo JR. CT evaluation of diffuse infiltrative lung disease: dose considerations and optimal technique. J Thorac Imaging 2009; 24:252–259.
7. Studler U, Gluecker T, Bongartz G, Roth J, Steinbrich W. Image quality from high-resolution CT of the lung: comparison of axial scans and of sections reconstructed from volumetric data acquired using MDCT. AJR Am J Roentgenol 2005; 185:602–607.
8. Bastos M, Lee EY, Strauss KJ, Zurakowski D, Tracy DA, Boiselle PM. Motion artifact on high-resolution CT images of pediatric patients: comparison of volumetric and axial CT methods. AJR Am J Roentgenol 2009; 193:1414–1418.
9. Funama Y, Awai K, Taguchi K, Hatemura M, Yanaga Y, Shimamura M, Yamashita Y. Cone-beam technique for 64-MDCT of lung: image quality comparison with stepwise (step-and-shoot) technique. AJR Am J Roentgenol 2009; 192:273–278.
10. Dodd JD, Souza CA, Müller NL. Conventional high-resolution CT versus helical high-resolution MDCT in the detection of bronchiectasis. AJR Am J Roentgenol 2006; 187:414–420.
11. Hill LE, Ritchie G, Wightman AJ, Hill AT, Murchison JT. Comparison between conventional interrupted high-resolution CT and volume multidetector CT acquisition in the assessment of bronchiectasis. Br J Radiol 2010; 83:67–70.
12. Deterding R. Evaluating infants and children with interstitial lung disease. Semin Respir Crit Care Med 2007; 28:333–341.
13. Long FR. High-resolution CT of the lungs in infants and young children. J Thorac Imaging 2001; 16:251–258.
14. Garcia-Peña P, Lucaya J. HRCT in children: technique and indications. Eur Radiol 2004; 14 Suppl 4:L13–L30.
15. Ritchie CJ, Godwin JD, Crawford CR, Stanford W, Anno H, Kim Y. Minimum scan speeds for suppression of motion artifacts in CT. Radiology 1992; 185:37–42.
16. de Jong PA, Nakano Y, Lequin MH, Tiddens HA. Dose reduction for CT in children with cystic fibrosis: is it feasible to reduce the number of images per scan? Pediatr Radiol 2006; 36:50–53.
17. Goris ML, Robinson TE. Sampling density for the quantitative evaluation of air trapping. Pediatr Radiol 2009; 39:221–225.
18. Choi SJ, Choi BK, Kim HJ, Lee SH, Choi SH, Park SJ, Goo HW, Lee JS, Yoon CH. Lateral decubitus HRCT: a simple technique to replace expiratory CT in children with air trapping. Pediatr Radiol 2002; 32:179–182.
19. Goo HW, Kim HJ. Detection of air trapping on inspiratory and expiratory phase images obtained by 0.3-second cine CT in the lungs of free-breathing young children. AJR Am J Roentgenol 2006; 187:1019–1023.
20. Tusman G, Böhm SH, Tempra A, Melkun F, García E, Turchetto E, Mulder PG, Lachmann B. Effects of recruitment maneuver on atelectasis in anesthetized children. Anesthesiology 2003; 98:14–22.
21. Long FR, Castile RG. Technique and clinical applications of full-inflation and end-exhalation controlled-ventilation chest CT in infants and young children. Pediatr Radiol 2001; 31:413–422.
22. Zhang J, Bruesewitz MR, Bartholmai BJ, McCollough CH. Selection of appropriate computed tomographic image reconstruction algorithms for a quantitative multicenter trial of diffuse lung disease. J Comput Assist Tomogr 2008; 32:233–237.
23. Owens C. Pearls and pitfalls in HRCT in children. Paediatr Respir Rev 2006; 7(Suppl 1):S44–S49.
24. Brody AS, Guillerman RP, Hay TC, Wagner BD, Young LR, Deutsch GH, Fan LL, Deterding RR. Neuroendocrine cell hyperplasia of infancy: diagnosis with high-resolution CT. AJR Am J Roentgenol 2010; 194:238–244.
25. Altes TA, Mata J, de Lange EE, Brookeman JR, Mugler JP III. Assessment of lung development using hyperpolarized helium-3 diffusion MR imaging. J Magn Reson Imaging 2006; 24:1277–1283.
26. Ochs M, Nyengaard JR, Jung A, Knudsen L, Voigt M, Wahlers T, Richter J, Gundersen HJ. The number of alveoli in the human lung. Am J Respir Crit Care Med 2004; 169:120–124.
27. Zompatori M, Sverzellati N, Poletti V, Bnà C, Ormitti F, Spaggiari E, Maffei E. High-resolution CT in diagnosis of diffuse infiltrative lung disease. Semin Ultrasound CT MR 2005; 26:332–347.
28. Hansell DM, Bankier AA, MacMahon H, McLoud TC, Müller NL, Remy J. Fleischner Society: glossary of terms for thoracic imaging. Radiology 2008; 246:697–722.
29. MacDonald S, Müller NL. Insights from HRCT: how they affect the management of diffuse parenchymal lung disease. Semin Respir Crit Care Med 2003; 24:357–364.
30. Johnson JL, Kramer SS, Mahboubi S. Air trapping in children: evaluation with dynamic lung densitometry with spiral CT. Radiology 1998; 206:95–101.

31. Stankiewicz P, Sen P, Bhatt SS, Storer M, Xia Z, Bejjani BA, Ou Z, Wiszniewska J, Driscoll DJ, Maisenbacher MK, Bolivar J, Bauer M, Zackai EH, McDonald-McGinn D, Nowaczyk MM, Murray M, Hustead V, Mascotti K, Schultz R, Hallam L, McRae D, Nicholson AG, Newbury R, Durham-O'Donnell J, Knight G, Kini U, Shaikh TH, Martin V, Tyreman M, Simonic I, Willatt L, Paterson J, Mehta S, Rajan D, Fitzgerald T, Gribble S, Prigmore E, Patel A, Shaffer LG, Carter NP, Cheung SW, Langston C, Shaw-Smith C. Genomic and genic deletions of the *FOX* gene cluster on 16q24.1 and inactivating mutations of FOXF1 cause alveolar capillary dysplasia and other malformations. Am J Hum Genet 2009; 84:780–791.
32. Michalsky MP, Arca MJ, Groenman F, Hammond S, Tibboel D, Caniano DA. Alveolar capillary dysplasia: a logical approach to a fatal disease. J Pediatr Surg 2005; 40:1100–1105.
33. Hugosson CO, Salama HM, Al-Dayel F, Khoumais N, Kattan AH. Primary alveolar capillary dysplasia (acinar dysplasia) and surfactant protein B deficiency: a clinical, radiological and pathological study. Pediatr Radiol 2005; 35:311–316.
34. Gillespie LM, Fenton AC, Wright C. Acinar dysplasia: a rare cause of neonatal respiratory failure. Acta Paediatr 2004; 93:712–713.
35. Newman B, Yunis E. Primary alveolar capillary dysplasia. Pediatr Radiol 1990; 21:20–22.
36. Agrons GA, Courtney SE, Stocker JT, Markowitz RI. From the archives of the AFIP: Lung disease in premature neonates: radiologic-pathologic correlation. Radiographics 2005; 25:1047–1073.
37. Mahut B, De Blic J, Emond S, Benoist MR, Jarreau PH, Lacaze-Masmonteil T, Magny JF, Delacourt C. Chest computed tomography findings in bronchopulmonary dysplasia and correlation with lung function. Arch Dis Child Fetal Neonatal Ed 2007; 92:F459–F464.
38. Biko DM, Schwartz M, Anupindi SA, Altes TA. Subpleural lung cysts in Down syndrome: prevalence and association with coexisting diagnoses. Pediatr Radiol 2008; 38:280–284.
39. Taylor PA, Dishop MK, Lotze TE, Mallory GB, Guillerman RP. Congenital multilobar emphysema: a characteristic lung growth disorder attributable to Filamin A gene mutations. Pediatr Radiol 2009;39(Suppl 3):S516.
40. Deterding RR, Pye C, Fan LL, Langston C. Persistent tachypnea of infancy is associated with neuroendocrine cell hyperplasia. Pediatr Pulmonol 2005; 40:157–165.
41. Deterding RR. Infants and young children with children's interstitial lung disease. Pediatric Allergy, Immunology, and Pulmonology 2010; 23:25–31.
42. Smets K, Dhaene K, Schelstraete P, Meersschaut V, Vanhaesebrouck P. Neonatal pulmonary interstitial glycogen accumulation disorder. Eur J Pediatr 2004; 163:408–409.
43. Onland W, Molenaar JJ, Leguit RJ, van Nierop JC, Noorduyn LA, van Rijn RR, Geukers VG. Pulmonary interstitial glycogenosis in identical twins. Pediatr Pulmonol 2005; 40:362–366.
44. Canakis AM, Cutz E, Manson D, O'Brodovich H. Pulmonary interstitial glycogenosis: a new variant of neonatal interstitial lung disease. Am J Respir Crit Care Med 2002; 165:1557–1565.
45. Lanfranchi M, Allbery SM, Wheelock L, Perry D. Pulmonary interstitial glycogenosis. Pediatr Radiol 2010; 40:361–365.
46. Bush A. Paediatric interstitial lung disease: not just kid's stuff. Eur Respir J 2004; 24:521–523.
47. Olsen E ØE, Sebire NJ, Jaffe A, Owens CM. Chronic pneumonitis of infancy: high-resolution CT findings. Pediatr Radiol 2004; 34:86–88.
48. Hamvas A. Inherited surfactant protein-B deficiency and surfactant protein-C associated disease: clinical features and evaluation. Semin Perinatol 2006; 30:316–326.
49. Soraisham AS, Tierney AJ, Amin HJ. Neonatal respiratory failure associated with mutation in the surfactant protein C gene. J Perinatol 2006; 26:67–70.
50. Prestridge A, Wooldridge J, Deutsch G, Young LR, Wert SE, Whitsett JA, Nogee L. Persistent tachypnea and hypoxia in a 3-month-old term infant. J Pediatr 2006; 149:702–706.
51. Stevens PA, Pettenazzo A, Brasch F, Mulugeta S, Baritussio A, Ochs M, Morrison L, Russo SJ, Beers MF. Nonspecific interstitial pneumonia, alveolar proteinosis, and abnormal proprotein trafficking resulting from a spontaneous mutation in the surfactant protein C gene. Pediatr Res 2005; 57:89–98.
52. Doan ML, Guillerman RP, Dishop MK, Nogee LM, Langston C, Mallory GB, Sockrider MM, Fan LL. Clinical, radiological and pathological features of ABCA3 mutations in children. Thorax 2008; 63:366–373.
53. Gordon IO, Cipriani N, Arif Q, Mackinnon AC, Husain AN. Update in nonneoplastic lung diseases. Arch Pathol Lab Med 2009; 133:1096–1105.
54. Griese M, Brasch F, Aldana VR, Cabrera MM, Goelnitz U, Ikonen E, Karam BJ, Liebisch G, Linder MD, Lohse P, Meyer W, Schmitz G, Pamir A, Ripper J, Rolfs A, Schams A, Lezana FJ. Respiratory disease in Niemann–Pick type C2 is caused by pulmonary alveolar proteinosis. Clin Genet 2010; 77:119–130.
55. Krude H, Schütz B, Biebermann H, von Moers A, Schnabel D, Neitzel H, Tönnies H, Weise D, Lafferty A, Schwarz S, DeFelice M, von Deimling A, van Landeghem F, DiLauro R, Grüters A. Choreoathetosis, hypothyroidism, and pulmonary alterations due to human NKX2-1 haploinsufficiency. J Clin Invest 2002; 109:475–480.
56. Albafouille V, Sayegh N, De Coudenhove S, Scheinmann P, De Blic J, Mamou-Mani T, Hassine A, Jaubert F, Brunelle F. CT scan patterns of pulmonary alveolar proteinosis in children. Pediatr Radiol 1999; 29:147–152.
57. Vrielynck S, Mamou-Mani T, Emond S, Scheinmann P, Brunelle F, de Blic J. Diagnostic value of high-resolution CT in the evaluation of chronic infiltrative lung disease in children. AJR Am J Roentgenol 2008; 191:914–920.
58. Copley SJ, Padley SP. High-resolution CT of paediatric lung disease. Eur Radiol 2001; 11:2564–2575.
59. Suzuki T, Sakagami T, Rubin BK, Nogee LM, Wood RE, Zimmerman SL, Smolarek T, Dishop MK, Wert SE, Whitsett JA, Grabowski G, Carey BC, Stevens C, van der Loo JC, Trapnell BC. Familial pulmonary alveolar proteinosis caused by mutations in CSF2RA. J Exp Med 2008; 205:2703–2710.
60. Martinez-Moczygemba M, Doan ML, Elidemir O, Fan LL, Cheung SW, Lei JT, Moore JP, Tavana G, Lewis LR, Zhu Y, Muzny DM, Gibbs RA, Huston DP. Pulmonary alveolar proteinosis caused by deletion of the GM-CSFRalpha gene in the X chromosome pseudoautosomal region 1. J Exp Med 2008; 205:2711–2716.
61. Parto K, Svedström E, Majurin ML, Härkönen R, Simell O. Pulmonary manifestations in lysinuric protein intolerance. Chest 1993; 104:1176–1182.
62. Santamaria F, Parenti G, Guidi G, Rotondo A, Grillo G, Larocca MR, Celentano L, Strisciuglio P, Sebastio G, Andria G. Early detection of lung involvement in lysinuric protein intolerance: role of high-resolution computed tomography and radioisotopic methods. Am J Respir Crit Care Med 1996; 153:731–735.
63. Chung CJ, Fordham LA, Barker P, Cooper LL. Children with congenital pulmonary lymphangiectasia: after infancy. AJR Am J Roentgenol 1999; 173:1583–1588.
64. Barker PM, Esther CR Jr., Fordham LA, Maygarden SJ, Funkhouser WK. Primary pulmonary lymphangiectasia in infancy and childhood. Eur Respir J 2004; 24:413–419.
65. Esther CR Jr., Barker PM. Pulmonary lymphangiectasia: diagnosis and clinical course. Pediatr Pulmonol 2004; 38:308–313.
66. Copley SJ, Coren M, Nicholson AG, Rubens MB, Bush A, Hansell DM. Diagnostic accuracy of thin-section CT and chest radiography of pediatric interstitial lung disease. AJR Am J Roentgenol 2000; 174:549–554.

67. Swensen SJ, Hartman TE, Mayo JR, Colby TV, Tazelaar HD, Müller NL. Diffuse pulmonary lymphangiomatosis: CT findings. J Comput Assist Tomogr 1995; 19:348–352.
68. Faul JL, Berry GJ, Colby TV, Ruoss SJ, Walter MB, Rosen GD, Raffin TA. Thoracic lymphangiomas, lymphangiectasis, lymphangiomatosis, and lymphatic dysplasia syndrome. Am J Respir Crit Care Med 2000; 161:1037–1046.
69. Frazier AA, Franks TJ, Mohammed TL, Ozbudak IH, Galvin JR. From the Archives of the AFIP: pulmonary veno-occlusive disease and pulmonary capillary hemangiomatosis. Radiographics 2007; 27:867–882.
70. Nicholson AG. Lymphocytic interstitial pneumonia and other lymphoproliferative disorders in the lung. Semin Respir Crit Care Med 2001; 22:409–422.
71. Bramson RT, Cleveland R, Blickman JG, Kinane TB. Radiographic appearance of follicular bronchitis in children. AJR Am J Roentgenol 1996; 166:1447–1450.
72. Becciolini V, Gudinchet F, Cheseaux JJ, Schnyder P. Lymphocytic interstitial pneumonia in children with AIDS: high-resolution CT findings. Eur Radiol 2001; 11:1015–1020.
73. Howling SJ, Hansell DM, Wells AU, Nicholson AG, Flint JD, Müller NL. Follicular bronchiolitis: thin-section CT and histologic findings. Radiology 1999; 212:637–642.
74. Pitcher RD, Beningfield SJ, Zar HJ. Chest radiographic features of lymphocytic interstitial pneumonitis in HIV-infected children. Clin Radiol 2010; 65:150–154.
75. Marks MJ, Haney PJ, McDermott MP, White CS, Vennos AD. Thoracic disease in children with AIDS. Radiographics 1996; 16:1349–1362.
76. Yalçin E, Dogru D, Haliloglu M, Ozçelik U, Kiper N, Göçmen A. Postinfectious bronchiolitis obliterans in children: clinical and radiological profile and prognostic factors. Respiration 2003; 70:371–375.
77. Zhang L, Irion K, da Silva Porto N, Abreu e Silva F. High-resolution computed tomography in pediatric patients with postinfectious bronchiolitis obliterans. J Thorac Imaging 1999; 14:85–89.
78. Moonnumakal SP, Fan LL. Bronchiolitis obliterans in children. Curr Opin Pediatr 2008; 20:272–278.
79. Lucaya J, Gartner S, García-Peña P, Cobos N, Roca I, Liñan S. Spectrum of manifestations of Swyer-James-MacLeod syndrome. J Comput Assist Tomogr 1998; 22:592–597.
80. Fan LL. Hypersensitivity pneumonitis in children. Curr Opin Pediatr 2002; 14:323–326.
81. Hartman TE. The HRCT features of extrinsic allergic alveolitis. Semin Respir Crit Care Med 2003; 24:419–426.
82. Susarla SC, Fan LL. Diffuse alveolar hemorrhage syndromes in children. Curr Opin Pediatr 2007; 19:314–320.
83. Fullmer JJ, Langston C, Dishop MK, Fan LL. Pulmonary capillaritis in children: a review of eight cases with comparison to other alveolar hemorrhage syndromes. J Pediatr 2005; 146:376–381.
84. Nuesslein TG, Teig N, Rieger CH. Pulmonary haemosiderosis in infants and children. Paediatr Respir Rev 2006; 7:45–48.
85. Ravenel JG, McAdams HP. Pulmonary vasculitis: CT features. Semin Respir Crit Care Med 2003; 24:427–436.
86. Koh DM, Hansell DM. Computed tomography of diffuse interstitial lung disease in children. Clin Radiol 2000; 55:659–667.
87. Connolly B, Manson D, Eberhard A, Laxer RM, Smith C. CT appearance of pulmonary vasculitis in children. AJR Am J Roentgenol 1996; 167:901–904.
88. Deniz O, Ors F, Tozkoparan E, Ozcan A, Gumus S, Bozlar U, Bilgic H, Ekiz K, Demirci N. High resolution computed tomographic features of pulmonary alveolar microlithiasis. Eur J Radiol 2005; 55:452–460.
89. Tachibana T, Hagiwara K, Johkoh T. Pulmonary alveolar microlithiasis: review and management. Curr Opin Pulm Med 2009; 15:486–490.
90. Kligerman SJ, Groshong S, Brown KK, Lynch DA. Nonspecific interstitial pneumonia: radiologic, clinical, and pathologic considerations. Radiographics 2009; 29:73–87.
91. Panigada S, Ravelli A, Silvestri M, Granata C, Magni-Manzoni S, Cerveri I, Dore R, Tomà P, Martini A, Rossi GA, Sacco O. HRCT and pulmonary function tests in monitoring of lung involvement in juvenile systemic sclerosis. Pediatr Pulmonol 2009; 44:1226–1234.
92. Seely JM, Jones LT, Wallace C, Sherry D, Effmann EL. Systemic sclerosis: using high-resolution CT to detect lung disease in children. AJR Am J Roentgenol 1998; 170:691–697.
93. Aaløkken TM, Lilleby V, Søyseth V, Mynarek G, Pripp AH, Johansen B, Førre O, Kolbenstvedt A. Chest abnormalities in juvenile-onset mixed connective tissue disease: assessment with high-resolution computed tomography and pulmonary function tests. Acta Radiol 2009; 50:430–436.
94. Fenlon HM, Doran M, Sant SM, Breatnach E. High-resolution chest CT in systemic lupus erythematosus. AJR Am J Roentgenol 1996; 166:301–307.
95. Lilleby C, Aalokeen TM, Johansen B, Førre Ø. Pulmonary involvement in patients with childhood-onset systemic lupus erythematosus. Clin Exp Rheumatol 2006; 24:203–208.
96. Keesling CA, Frush DP, O'Hara SM, Fordham LA. Clinical and imaging manifestations of pediatric sarcoidosis. Acad Radiol 1998; 5:122–132.
97. Milman N, Hoffmann AL, Byg KE. Sarcoidosis in children. Epidemiology in Danes, clinical features, diagnosis, treatment and prognosis. Acta Paediatr 1998; 87:871–878.
98. Fan LL, Deterding RR, Langston C. Pediatric interstitial lung disease revisited. Pediatr Pulmonol 2004; 38:369–378.
99. Polverosi R, Maffesanti M, Dalpiaz G. Organizing pneumonia: typical and atypical HRCT patterns. Radiol Med 2006; 111:202–212.
100. Zanetti G, Marchiori E, Gasparetto TD, Escuissato DL, Soares Souza A Jr. Lipoid pneumonia in children following aspiration of mineral oil used in the treatment of constipation: high-resolution CT findings in 17 patients. Pediatr Radiol 2007; 37:1135–1139.
101. Marchiori E, Zanetti G, Mano CM, Irion KL, Daltro PA, Hochhegger B. Lipoid pneumonia in 53 patients after aspiration of mineral oil: comparison of high-resolution computed tomography findings in adults and children. J Comput Assist Tomogr 2010; 34:9–12.
102. Jeong YJ, Kim KI, Seo IJ, Lee CH, Lee KN, Kim KN, Kim JS, Kwon WJ. Eosinophilic lung diseases: a clinical, radiologic, and pathologic overview. Radiographics 2007; 27:617–37; discussion 637.
103. Oermann CM, Panesar KS, Langston C, Larsen GL, Menendez AA, Schofield DE, Cosio C, Fan LL. Pulmonary infiltrates with eosinophilia syndromes in children. J Pediatr 2000; 136:351–358.
104. Ha SY, Helms P, Fletcher M, Broadbent V, Pritchard J. Lung involvement in Langerhans' cell histiocytosis: prevalence, clinical features, and outcome. Pediatrics 1992; 89:466–469.
105. Odame I, Li P, Lau L, Doda W, Noseworthy M, Babyn P, Weitzman S. Pulmonary Langerhans cell histiocytosis: a variable disease in childhood. Pediatr Blood Cancer 2006; 47:889–893.
106. Junewick JJ, Fitzgerald NE. The thymus in Langerhans' cell histiocytosis. Pediatr Radiol 1999; 29:904–907.
107. McHugh K, Olsen E ØE, Vellodi A. Gaucher disease in children: radiology of non-central nervous system manifestations. Clin Radiol 2004; 59:117–123.
108. Goitein O, Elstein D, Abrahamov A, Hadas-Halpern I, Melzer E, Kerem E, Zimran A. Lung involvement and enzyme replacement therapy in Gaucher's disease. QJM 2001; 94:407–415.
109. Guillemot N, Troadec C, de Villemeur TB, Clément A, Fauroux B. Lung disease in Niemann–Pick disease. Pediatr Pulmonol 2007; 42:1207–1214.

110. Lynch DA, Hay T, Newell JD Jr., Divgi VD, Fan LL. Pediatric diffuse lung disease: diagnosis and classification using high-resolution CT. AJR Am J Roentgenol 1999; 173:713–718.
111. Schneebaum N, Blau H, Soferman R, Mussaffi H, Ben-Sira L, Schwarz M, Sivan Y. Use and yield of chest computed tomography in the diagnostic evaluation of pediatric lung disease. Pediatrics 2009; 124:472–479.
112. Nogee LM. Genetic basis of children's interstitial lung disease. Pediatric Allergy, Immunology, and Pulmonology 2010; 23:15–24.
113. Brody AS. New perspectives in imaging interstitial lung disease in children. Pediatr Radiol 2008; 38(Suppl 2):S205–S207.
114. Mattiello R, Sarria EE, Mallol J, Fischer GB, Mocelin H, Bello R, Flores JA, Irion K, Jones Y. Post-infectious bronchiolitis obliterans: Can CT scan findings at early age anticipate lung function? Pediatr Pulmonol 2010; 45:315–319.
115. Wells AU. High-resolution computed tomography in the diagnosis of diffuse lung disease: a clinical perspective. Semin Respir Crit Care Med 2003; 24:347–356.

Address correspondence to:
R. Paul Guillerman, M.D.
Diagnostic Imaging Services
Texas Children's Hospital
6621 Fannin CC470.01
Houston, TX 77030

E-mail: rpguille@texaschildrens.org

Received for publication March 21, 2010; accepted after revision March 22, 2010